Dissecting Porosity in Molecular Crystals: Influence of Geometry, Hydrogen Bonding, and [#···#] Stacking on the Solid-State Packing of Fluorinated Aromatics

Mohamed Isameldin Hashim, Ha T. M. Le, Teng-Hao Chen, Yu-Sheng Chen, Olafs Daugulis, Chia-Wei Hsu, Allan J Jacobson, Watchareeya Kaveevivitchai, Xiao Liang, Tatyana Makarenko, Ognjen Š. Miljani#, Ilja Popovs, Hung Vu Tran, Xiqu Wang, Chia-Hua Wu, and Judy I. Wu

J. Am. Chem. Soc., **Just Accepted Manuscript** • DOI: 10.1021/jacs.8b02869 • Publication Date (Web): 14 Apr 2018

Dissecting Porosity in Molecular Crystals: Influence of Geometry, Hydrogen Bonding, and [π···π] Stacking on the Solid-State Packing of Fluorinated Aromatics

Mohamed I. Hashim,† Ha T. M. Le,† Teng-Hao Chen,† Yu-Sheng Chen,‡ Olafs Daugulis,† Chia-Wei Hsu,† Allan J. Jacobson,†,§ Watchareeya Kaveevivitchai,† Xiao Liang,† Tatyana Makarenko,† Ognjen Š. Miljanić,†,* Ilja Popovs,† Hung Vu Tran,† Xiqu Wang,† Chia-Hua Wu,† and Judy I. Wu†

† University of Houston, Department of Chemistry, 3585 Cullen Boulevard #112, Houston TX, 77204-5003, USA

‡ Center for Advanced Radiation Source (ChemMatCARS), The University of Chicago, c/o APS/ANL, 9700 South Cass Drive, Argonne, IL 60439, USA

§ Texas Center for Superconductivity, 202 UH Science Center, Houston, TX 77204-5002, USA

ABSTRACT: Porous molecular crystals are an emerging class of porous materials that is unique in being built from discrete molecules rather than being polymeric in nature. In this study, we examined the effects of molecular structure of the precursors on the formation of porous solid-state structures with a series of sixteen rigid aromatics. The majority of these precursors possess pyrazole groups capable of hydrogen bonding and a combination of electron-rich aromatics and electron-poor tetrafluorobenzene rings. These precursors were prepared using a combination of Pd- and Cu-catalyzed cross-couplings, careful manipulations of protecting groups on the nitrogen atoms, and solvothermal syntheses. Our study varied the geometry and dimensions of precursors, as well as the presence of groups capable of hydrogen bonding and [π···π] stacking. Thirteen derivatives were crystallographically characterized, and four of them were found to be porous with surface areas between 259 and 1,159 $m^2 g^{-1}$. Common to these four porous structures were: (*a*) rigid trigonal geometry, (*b*) [π···π] stacking of electron-oor tetrafluorobenzenes with electron-rich pyrazoles or tetrazoles, and (*c*) hydrogen bonding between the terminal heteroaromatic rings.

INTRODUCTION

Porous materials,[1] such as zeolites, metal-organic frameworks (MOFs),[2] and covalent organic frameworks (COFs),[3] have myriads of applications in gas storage and separations, catalysis, fuel processing, and other areas. These three established classes of porous materials are all extended polymeric structures.[4] Such polymeric nature enhances their stability and robustness, but also makes their manufacture into films and devices more challenging—since these materials lack solution- and vapor-phase processability.[5] In addition, the inaccessibility of solution-phase characterization and processing techniques makes synthetic modifications and mechanistic investigations quite difficult.

Porous molecular crystals[6] are, in contrast, built from discrete molecules that pack in the solid state with large voids. Their porosity can be *extrinsic*—wherein the pores are a product of crystal packing, or *intrinsic*—which are typically formed from macrocyclic and cage molecules which already contain a void in their structures.[6d] Intrinsically porous molecular crystals have been constructed from cages based on boroxine,[7] imine,[8] hydrocarbon,[9] and benzoin[10] linkages. Extrinsically porous structures have been studied by the groups of Mastalerz—who used triptycenes[11] and other three-fold symmetric building blocks,[12] and Chen[13]—who relied on the hydrogen bonding 2,4-diaminotriazinyl (DAT)[14] group. Extrinsically porous structures based on guanine tetramers were recently reported.[15] Both classes offer promise of unique solution and vapor-phase processability which could open this class of materials to applications in membranes,[16] proton conductivity,[17] separations,[18] switchable porosity,[19] quartz crystal microbalance sensing,[20] as well as in the preparation of porous liquids[21] and organic alloys.[22]

In 2014, we have reported that the trigonal, extensively fluorinated pyrazole **1** (Figure 1) self-assembles into a solid-state structure with large voids.[23] This completely organic porous framework has a surface area of 1,159 $m^2 g^{-1}$ and is held together by a combination of [N–H···N] hydrogen bonds between the terminal pyrazole rings[24] and [π···π] stacking between the electron-rich pyrazoles and the electron-poor tetrafluorobenzene moieties. Crystals of this framework are lightweight, structurally stable up to 280 °C, and resistant to moisture, dilute acids and bases. This material is an effective adsorbent for hydrocarbons, potent greenhouse gases such as chlorofluorocarbons (CFCs) and fluorocarbons, as well as fluorinated anesthetics.[25] Furthermore, its solid-state structure is flexible and responsive to guest binding, suggesting it can be used as a piezochromic sensor for adsorbate binding.[26]

Discovery of the porous structure of **1** was serendipitous: compound **1** was initially developed as a ligand for fluorinated MOFs,[27] but attempts to coordinate it to a metal failed, yielding instead crystals of **1**—which revealed themselves as porous. In this contribution, we report a systematic dissection of the structure of **1**, which was undertaken with the intention of elucidating the exact elements of its molecular structure responsible for the formation of porous solid-state structure. The effects of changes in geometry and in hydrogen bonding and [π···π] stacking patterns were exam-

ined by synthesizing and crystallographically analyzing fifteen derivatives of **1**. During the course of this study, three new porous molecular crystals have been identified.

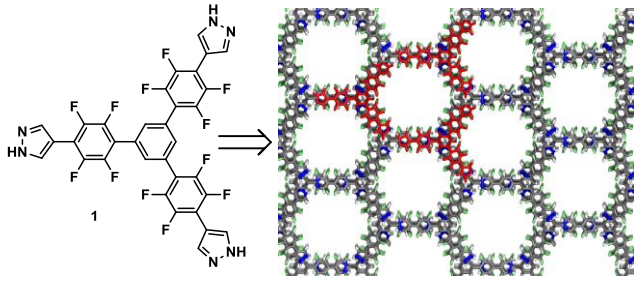

Figure 1. Rigid aromatic fluorinated trispyrazole **1** (left) crystalizes in a porous structure with one-dimensional channels (diameter: 16.5 Å) protruding through a three-dimensional crystal (right). Three neighboring molecules of **1** have been highlighted in red. Element colors for this and all other crystal structures in this article: C—gray, F—lime, N—blue, H—white.

RESULTS AND DISCUSSION

Design and Synthesis of Precursors[28]

The selection of potential candidates for self-assembly into porous solid-state structures was made with the intention of probing the effects of changing: (*a*) the shape and/or the length, (*b*) the hydrogen bonding capacity, or (*c*) the [π···π] stacking affinity of the three "arms" of **1**. Geometry changes were probed first through the synthesis of linear, bent, and other triangular analogs of **1**. Linear analogs **2**–**6**, whose synthesis is shown in Scheme 1, were designed with both the hydrogen-bonding pyrazole termini and the 1,2,4,5-tetrafluorobenzene moieties needed for aromatic stacking; what varied was their length (**2**–**4**), twisting between the aromatic rings (**5**), and dynamic nature of the imine connectors (**6**).

Starting with *N*-trityl protected iodopyrazole **7**,[23,29] Pd-catalyzed (and Cu-promoted) coupling with 1,2,4,5-tetrafluorobenzene resulted in versatile intermediate **8**.[23] The reaction of **8** with two 1,4-diiodobenzene derivatives generated linear precursors with three phenyl rings separating the two pyrazole moieties. Both of these materials were then subjected to a three-step synthetic sequence: (*a*) their *N*-trityl group was removed and (*b*) replaced with the thermolabile *tert*-butyloxycarbonyl (Boc) group, which was then itself (*c*) slowly cleaved under solvothermal conditions (DMF/MeOH/80 °C/24 h)[30] in the last step of the sequence, ultimately generating **4** (as cubic crystals) and **5** (as sea urchin-like crystals). This three-step sequence of manipulations of the protecting groups on nitrogen was used at the end of almost all precursors' syntheses. It was necessary as the Boc group would have been cleaved at high temperatures employed in the C–C coupling steps, and had to be installed at the very end of the synthesis—and then slowly cleaved to yield single crystalline materials.

Reacting two equivalents of **7** with 1,2,4,5-tetrafluorobenzene, followed by the same manipulation of *N*-protecting groups described for **4**/**5**, resulted in compound **2**, while the application of the same sequence of steps on 2,2',3,3',5,5',6,6'-octafluoro-1,1'-biphenyl ultimately produced **3**. Crystals of **2** and **3** were produced under solvothermal conditions, by heating the *N*-Boc protected precursors in a mixture of DMF and MeOH.

The linear diimine **6** was designed as a potentially self-assembling precursor to porous molecular crystals, which would come together through the reaction of perfluorinated terephthaldehyde **9** with two equivalents of 3-chloro-1H-pyrazol-4-amine. Yellow crystals of **6** were formed after heating the two precursors in EtOH at reflux for 12 h.

Scheme 1. Synthesis of linear precursors 2–6.

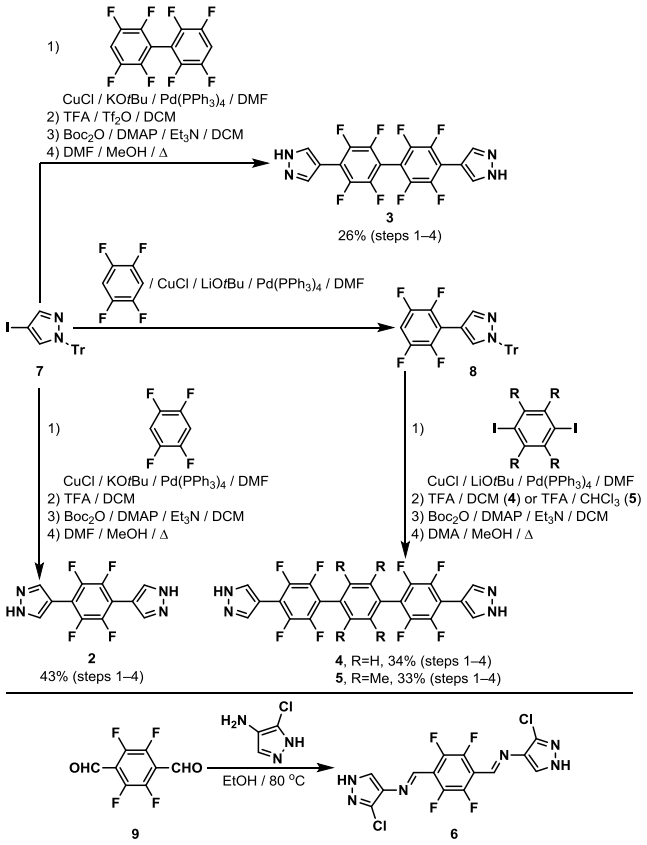

The bent precursors **10** and **11** were synthesized analogously to their linear counterparts (Scheme 2). Starting with **8**, reaction with 1,3-diiodobenzene was followed by the cleavage of *N*-trityl group, installation of the Boc group, and its ultimate solvothermal cleavage, resulting in **10**. The unsymmetrical precursor **11** was prepared starting from 3-iodobromobenzene, whose more reactive iodine substituent was first engaged into the reaction with **8** to give intermediate **12**. Compound **12** was then subjected to bromine-iodine exchange to produce **13**, which was reacted with extensively fluorinated biphenyl precursor **14**. A final series of manipulations of the protecting groups on the pyrazole nitrogens ensued, giving the bent compound **11**. Single crystals of **10** and **11** were produced in the last solvothermal step, in a fashion analogous to **2**–**4**.

Scheme 2. Synthesis of bent precursors 10 and 11.

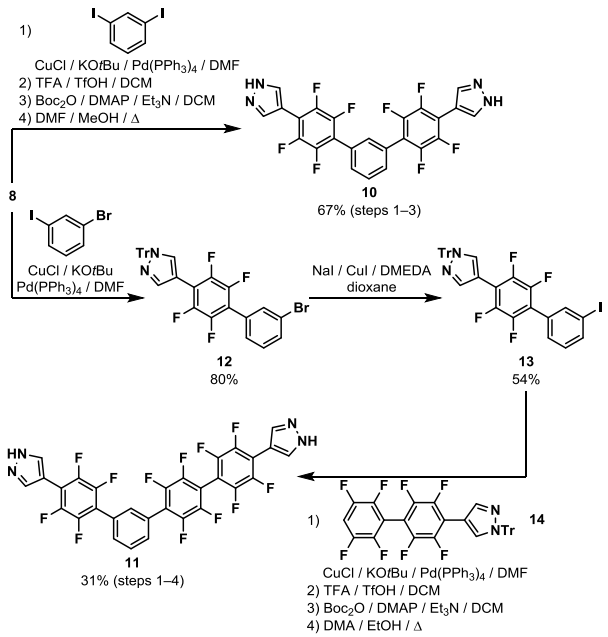

Trigonal pyrazole precursors **1** and **15** were also synthesized from **8**, by coupling it with 1,3,5-triiodobenzene (en route to **1**)[23] and 1,3,5-triiodo-2,4,6-trimethylbenzene (en route to **15**). The above-described three-step manipulation of functionalities on pyrazole nitrogens yielded **1** and **15** (Scheme 3, top). Compound **16**, characterized by the central 1,3,5-triazine core, was prepared differently (Scheme 3, bottom): first, fluorinated benzonitrile **17**[31] was trimerized into **18**, which was then coupled with **7** to create the skeleton of **16**. Manipulations of the *N*-protecting groups produced single crystals of the free **16** after the final solvothermal step.[32]

Scheme 3. Synthesis of trigonal pyrazoles 1, 15, and 16.

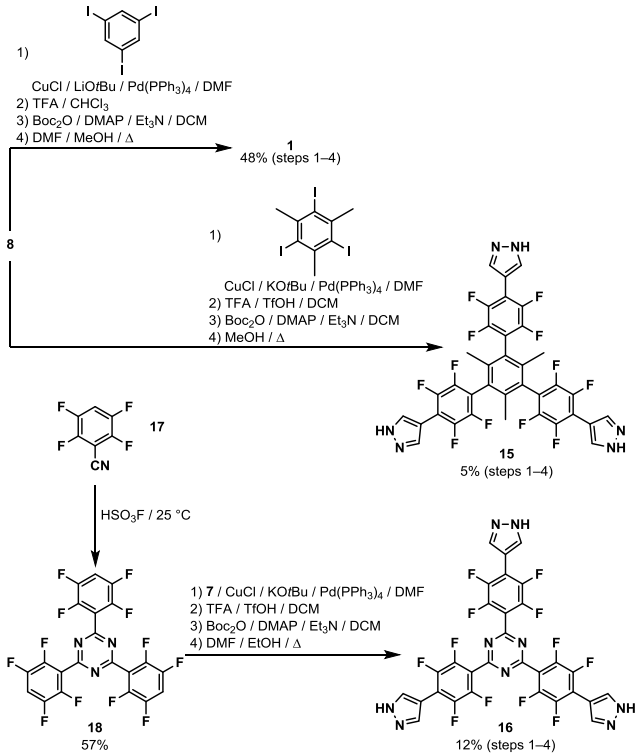

Scheme 4. Synthesis of precursors 19 and 20.

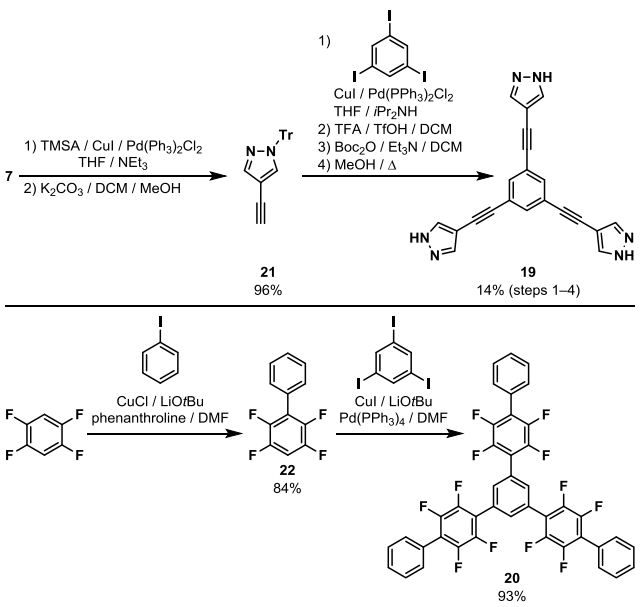

To explore the relative importance of hydrogen bonding and aromatic stacking interactions in the assembly of porous structures, we prepared compounds **19** and **20** (Scheme 4). The former was capable of hydrogen bonding, but not aromatic stacking, while the latter lacked the terminal groups capable of hydrogen bonding. The syntheses of **19** and **20** are shown in Scheme 4. A Sonogashira coupling of **7** with trimethylsilylacetylene (TMSA) and the subsequent cleavage of the silyl group generated terminal alkyne **21**. Its threefold Sonogashira coupling with 1,3,5-triiodobenzene was followed by the previously described three-step manipulation of nitrogen-protecting groups to finally yield the single crystals of **19** after the solvothermal Boc-group deprotection. Nonpolar **20** was easily prepared by a double C–H activation of 1,2,4,5-tetrafluorobenzene: first with iodobenzene to give **22,** and then with 1,3,5-triiodobenzene to yield **20**. Single crystals of **20** were obtained by the slow evaporation of its solution in THF.

Scheme 5. Synthesis of tristetrazole 23.

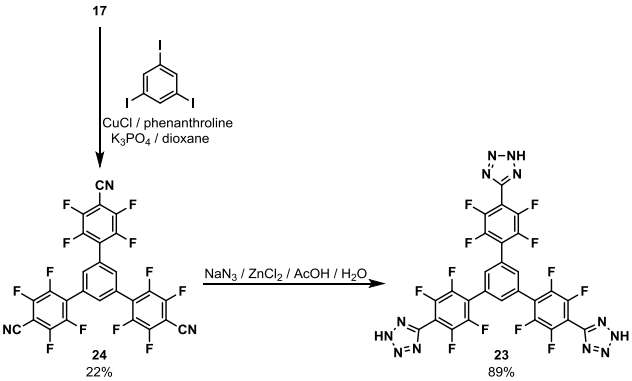

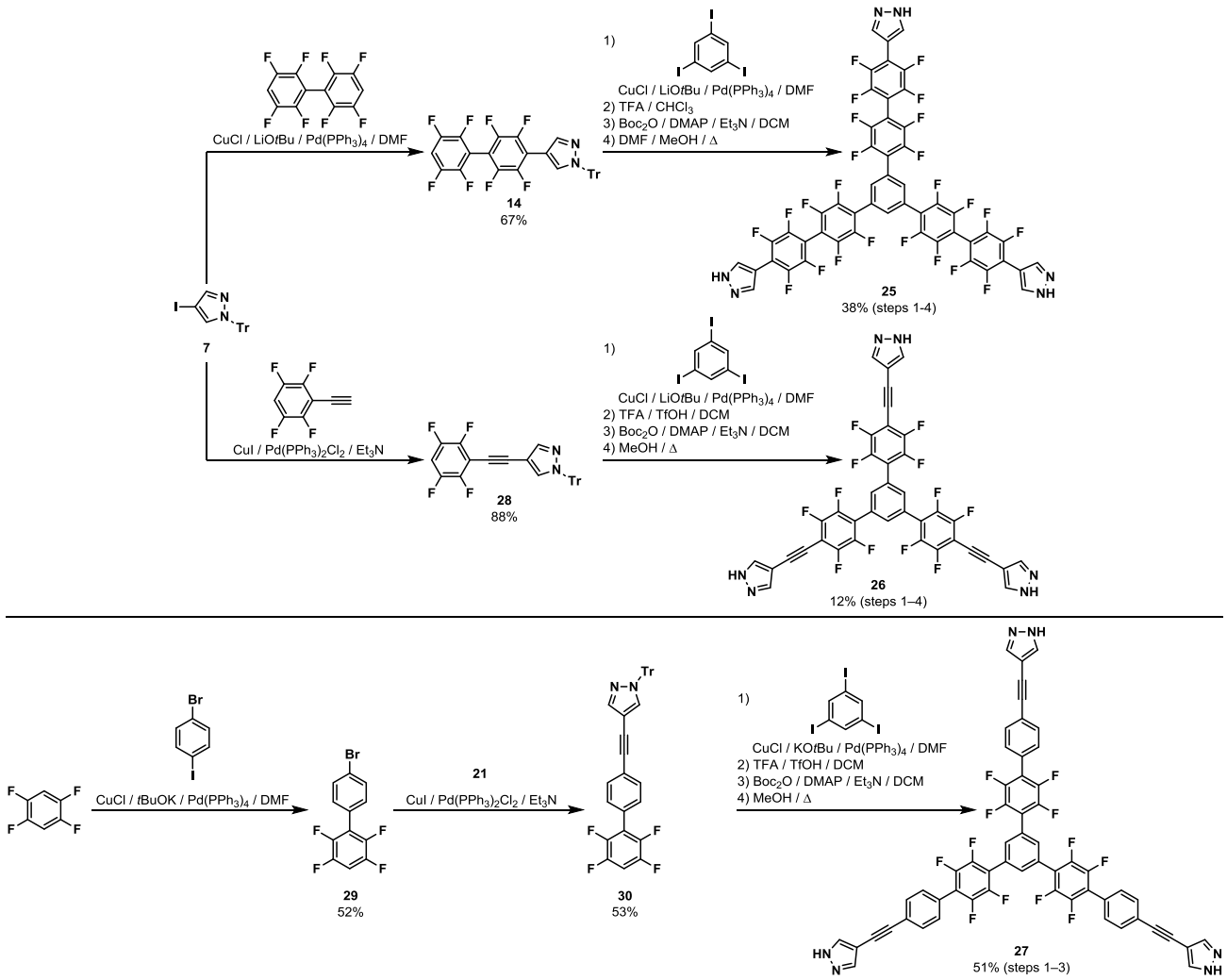

Scheme 6. Synthesis of elongated trigonal pyrazoles 25–27.

In addition to probing the effects of the removal of hydrogen bonding termini, we also examined the consequences of their change from pyrazoles to tetrazoles. This was explored through precursor **23**, which was synthesized from **17** in a two-step sequence which begun with a threefold coupling of **17** and 1,3,5-triiodobenzene and ended with a 1,3-dipolar reaction of the nitrile groups with azide in the presence of $ZnCl_2$, to yield **23** in 20% overall yield (Scheme 5).[27a] Single crystals of **23** were grown by the slow evaporation of its solution in a mixture of PhMe and MeOH.

The final group of compounds **25**–**27** (Scheme 6) involved elongating each of the trigonal arms of **1**. In each of them, the tetrafluorobenzene/pyrazole motif was retained, but the two moieties were separated by an electron-poor (in **25**) or electron-rich (in **26** and **27**) spacers. The synthesis of **25** and **26** commenced with **7**, which was either arylated into **14** or alkynylated into **28**. Both **14** and **28** were then subjected to an identical four-step sequence: (*a*) arylation of the fluorinated ring with 1,3,5-triiodobenzene; (*b*) cleavage of the *N*-trityl group; (*c*) installation of the Boc group, and finally (*d*) solvothermal cleavage of the Boc group, to give single crystals of **25** (from **14**, in DMF/MeOH mixture) and **26** (from **28**). The largest candidate compound **27** was prepared from 1,2,4,5-tetraflurobenzene, which was arylated to give **29**. The bromine functionality of compound **29** was subjected to a Sonogashira coupling with **21**, and the resulting product **30** was then reacted with 1,3,5-triiodobenzene. Standard manipulation of protecting groups on the nitrogen finally gave **27**.

Crystallographic Analysis

Linear Precursors. The crystal structure of **2**, shown in Figure 2, reveals an essentially planar molecule (angles between the planes of the central and terminal rings are 5.4°). Pyrazoles on each side of the molecule form catemers: infinite zig-zagging arrays of hydrogen bonds (N–H···N distance of 1.88 Å,[33] NHN angle 174°), wherein each molecule of **2** connects to four other molecules in the solid state (Figure 2A). Neighboring molecules of **2** are in planes that define a 54.4 ° angle; overall, the molecule organizes into corrugated 2D sheets (Figure 2B), which then stack on top of each other, resulting in an overall structure without observable pores.

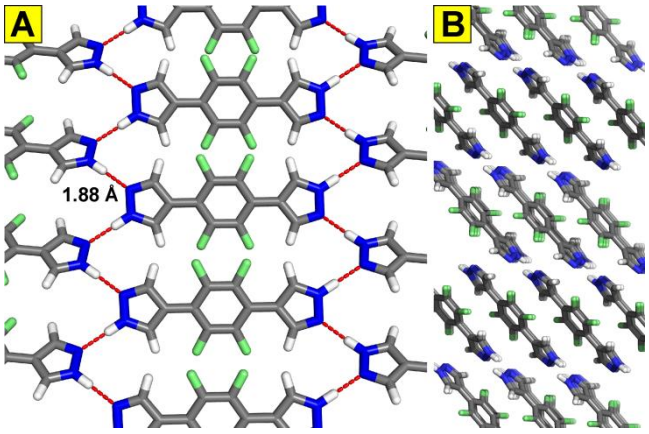

Figure 2. Crystal structure of compound **2**. Hydrogen bonding pattern organizes the molecules into a corrugated 2D sheet (**A**), which then stack (**B**) to produce the nonporous 3D structure.

Compound **3** is chemically very similar to **2**, but its molecular structure is much more deplanarized (Figure 3A). The two pyrazole rings are slightly distorted away from coplanarity with their tetrafluorobenzene neighbors (by 5.8 and 14.3 °). The largest distortion, however, is found in the deplanarization of the two 1,2,4,5-tetrafluorobenzene rings by 56.4 ° relative to each other. Similarly to **2**, each molecule of **3** connects to four of its neighbors via hydrogen bonding (N–H···N distances of 1.82 and 1.94 Å, NHN angles of 158 and 170 °, respectively). Just like in the case of **2**, stacking of these corrugated 2D sheets leaves no empty space in three-dimensional space, resulting in an overall nonporous structure. In both **2** and **3**, [π···π] stacking between pyrazoles and 1,2,4,5-tetrafluorobenzene moieties in not observable in the solid state.

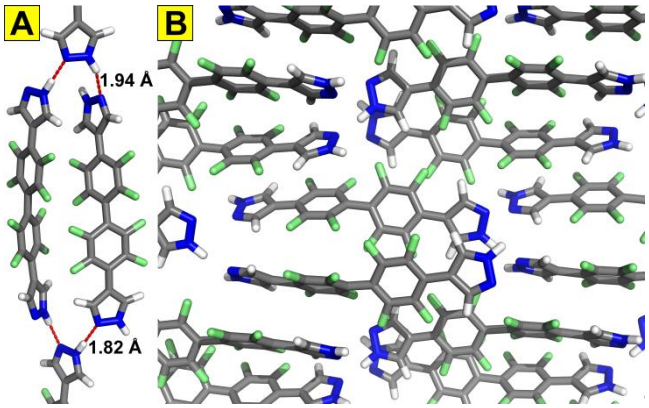

Figure 3. Crystal structure of compound **3**. Severely deplanarized molecules establish hydrogen bonds with their neighbors (**A**), resulting in a nonporous overall structure (**B**).

Crystals of compound **4** diffracted poorly and a satisfactory crystal structure could not be obtained. Preliminary structure (Supporting Information, Figure 68) revealed catemers very similar to those observed for **2** and apparent [π···π] stacking between pyrazole and tetrafluorobenzene functionalities. Nevertheless, the solid-state organization of **4** leaves no observable voids.[34] Nonfluorinated analogs of **2** and **3** form catemers as well.[28b,c]

In the solid-state structure of **5** (Figure 4A), four out of five aromatic rings are almost coplanar, with pyrazole/1,2,4,5-tetrafluorobenzene angles of 16.5 °. As expected, the central tetramethylated benzene ring is distorted from coplanarity with its perfluorinated neighbors by 67.2 °. Crystal structure of **5** stands out as the only one in the linear series with an incorporated ordered molecule of solvent, (MeOH). This causes the pyrazole N–H groups not to hydrogen bond to N atoms from other pyrazoles, but instead to the O atom of MeOH. Methanol's O–H group bridges the gap to the next pyrazole nucleus by establishing a hydrogen bond with its N atom. Resulting is an infinite 1D chain of pyrazole/MeOH/pyrazoles; parallel packing of these in the solid state (Figure 4) leaves no noticeable voids.

The crystal structure of the final linear precursor, diimine **6** (Supporting Information, Figure 69) revealed a molecule close to planarity, with the two imine groups oriented *anti* to each other. The hydrogen bonding pattern observed in the solid state structure of **6** is different from all the previously discussed analogs; pyrazole N–H group establishes an elongated hydrogen bond with the imine nitrogen (N–H···N distance of 1.89 Å, NHN angle of 159 °), while the pyrazole nitrogen forms bifurcating short contacts with the C–H groups of the imine (2.68 Å) and pyrazole (2.25 Å) in the neighboring molecule of **6**. Molecules of **6** also [π···π] stack with each other (Supporting Information, Figure 69B), with the 3.39 Å distance between the centroid of 1,2,4,5-tetrafluorobenzene ring and the averaged plane of the pyrazole ring. Nevertheless, the overall herringbone packing pattern means that **6** also forms a nonporous 3D structure.

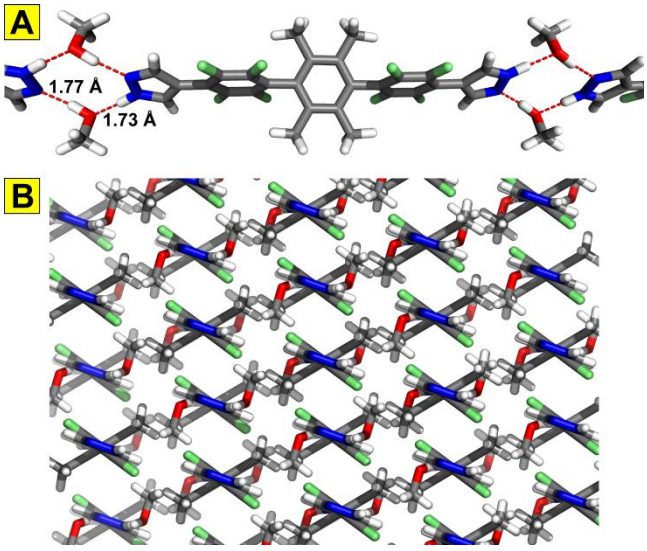

Figure 4. Crystal structure of compound **5**. Infinite hydrogen bonded chains of alternating molecules of **5** and MeOH (**A**) run parallel to each other in the nonporous 3D structure (**B**). Oxygen atoms shown in red.

In summary, none of the five linear precursors we analyzed has a porous crystal structure. Four out of five compounds had significant differences in the patterns of either hydrogen bonding or [π···π] stacking relative to prototype **1**. However, even compound **4**—which showed both hydrogen bonding and [π···π] stacking in the solid state—was nonporous, suggesting that the linear geometry may not be suitable for the formation of porous structures. We next turned our attention to bent precursors **10** and **11**.

Bent Precursors. The key features of the crystal structure of bent compound **10** are shown in Figure 5. The molecule crystallizes with a disordered molecule of DMF at half occupancy. The planes of the central benzene and neighboring 1,2,4,5-tetrafluorobenzene rings define angles of 49.8 °, while the fluorinated rings reside at a 18.6 ° angle relative to the pyrazole rings. In spite of resemblance in the molecular structure between **11** and **1**—the latter is essentially **1** with one arm removed—their hydrogen bonding patterns are quite different. While in **1** a triplet of hydrogen bonds between neighboring pyrazoles was observed, in the solid-state structure of **10** four pyrazoles hydrogen bonded into a quartet instead (Figure 5A), with N–H···N distances of 1.88 Å and 1.89 Å. There is also some evidence of [π···π] stacking in the crystal structure of **10** (Figure 5B), as reflected by distances between the plane of the fluorinated ring in one molecule and centroids of both the fluorinated (3.37 Å) and pyrazole (3.34 Å) ring in its neighboring molecule. However, the overall structure is interwoven in a way that leaves no sizable voids.

We were also successful in growing a single crystal of compound **11** suitable for X-ray diffraction experiments. Initial results revealed that there are no pores in this crystal structure; therefore, the experiment was discontinued and full crystal structure of **11** was not obtained.

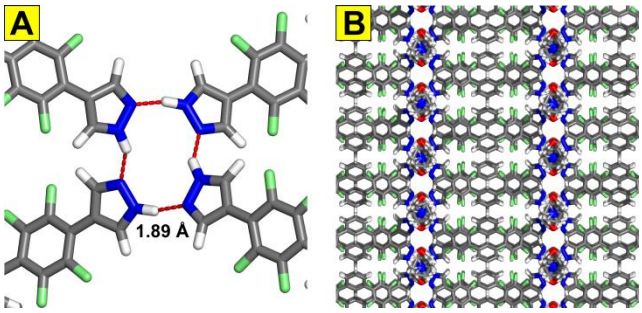

Figure 5. Crystal structure of bent precursor **10**. **A**—Four pyrazoles come together, forming a quartet of hydrogen bonds. **B**—Interweaving network seen along the crystallographic *b* axis.

Trigonal Precursors. After the somewhat disappointing results we have observed with linear and bent precursors, we turned to trigonally shaped compounds. Compounds **16**, introduced in Scheme 3, was examined first (despite extensive experimentation, single crystals of compound **15** could not be obtained). Crystals of **16** were suitable for X-ray diffraction and revealed a structure very similar to that of **1**; the two are shown side-by-side in Figure 6 (panels A–D for **1**, and E–H for **16**). The two compounds are remarkably isostructural. Both show twisting between the central trigonal ring and tetrafluorobenzenes (Figure 6A and 6E; interplanar angles of 36.8–49.5 ° in **1** and 32.3–46.0 ° in **16**), and tetrafluorobenzenes almost coplanar with terminal pyrazoles (interplanar angles of 10.1–12.6 ° in **1** and 9.8–11.5 ° in **16**). Both establish triplets of hydrogen bonds, shown in Figure 6B and 6F. Both also form infinite head-to-tail [π···π] stacks between tetrafluorobenzenes and pyrazoles (Figure 6C and 6G), characterized by the 3.44–3.47 (in **1**) and 3.38 (in **16**) Å distances between pyrazole centroids and averaged planes of tetrafluorobenzenes. Finally, this combination of stabilizing intermolecular interations results in porous networks in both cases (Figure 6D and 6H), with hexagonal pores of 16.5 and 15.8 Å diameters. Such remarkable similarity of the two structures bodes well for the preparation of porous organic alloys.[22]

While similar, **1** and **16** are not the same in all respects: because of the absence of hydrogen atoms on the central ring in **16**, the rotation of tetrafluorobenzenes around the C–C bonds connecting them to the central ring is less encumbered in **16** than in **1**. This feature has important consequences for the emission behavior of the two molecules. In the solid state, they are both emissive, with similar λ_{max} values (**1**: 382 nm; **16**: 371 nm). In dilute DMF solutions, however, their optical properties differ: the more rigid **1** remains emissive while the flexible **16** does not emit. However, the addition of H_2O to the DMF solutions of the latter rigidifies **16** as well, turning on its aggregation-induced emission (AIE).[32]

Alkyne-based compound **19** was studied to examine the effects of the removal of the electron-poor aromatic fragment on the [π···π] stacking patterns. Its crystal structure (Supporting Information, Figure 70A) reveals a slightly bent molecule whose C≡C–C angles ranged from 174.4 to 179.1 °. The three peripheral pyrazoles defined angles between 10.5 and 21.0 ° degrees with the planes of the central benzene ring. Molecules of **19** are similar to other triangular counterparts in that they also establish triplets of hydrogen bonds between pyrazoles (Supporting Information, Figure 70B), with N–H···N distances in the 1.82–1.89 Å range. However, the absence of the [π···π] stacking and the overall flexibility of these molecules results in the closely packed structure (Supporting Information, Figure 70C), in which undulating hydrogen bonded sheets of **19** weave in an offset fashion that leaves essentially no void spaces (as estimated by CSD Mercury software, with 1.0 Å probe radius).

In compound **20**, which was designed to be incapable of hydrogen bonding, the three tetrafluorobenzene rings define angles of 44.6, 44.6, and 49.0 ° with the plane of the central benzene ring (Supporting Information, Figure 71A). The peripheral benzene rings are, in contrast, almost coplanar with the central one, with small distortions in the 3.2–7.6 ° range. Two of the three peripheral benzene rings engage in [π···π] stacking with the tetrafluorobenzene, with their centroid being 3.51 Å from its averaged plane (Supporting Information, Figure 71B). However, overall crystal packing still leaves no voids, as shown in Supporting Information, Figure 71C.

Tetrazole-based compound **23** crystallizes with one disordered molecule of MeOH per molecule of **23**. Collection of sufficiently high quality diffraction data on **23** required the utilization of synchrotron radiation. Molecules of **23** are again deplanarized, as shown in Figure 7A; the propeller-like molecules have a threefold rotation axis, and the torsion angles between the central ring and three tetrafluorobenzenes are all 53.0 °; corresponding interplanar angles between tetrafluorobenzenes and tetrazoles are 35.8 °. Each tetrazole established two hydrogen bonds with its vertical neighbors, with N–H···N distances of 1.84 Å, resulting in overall stacks of molecules (Figure 7B). Within those stacks, the planes of central benzene rings from neighboring molecules are parallel to each other, and separated by 4.97 Å. This relationship seems to be an artefact of crystal packing and not indicative of [π···π] stacking. However, the arrangement of the twisted tetrafluorobenzene rings in

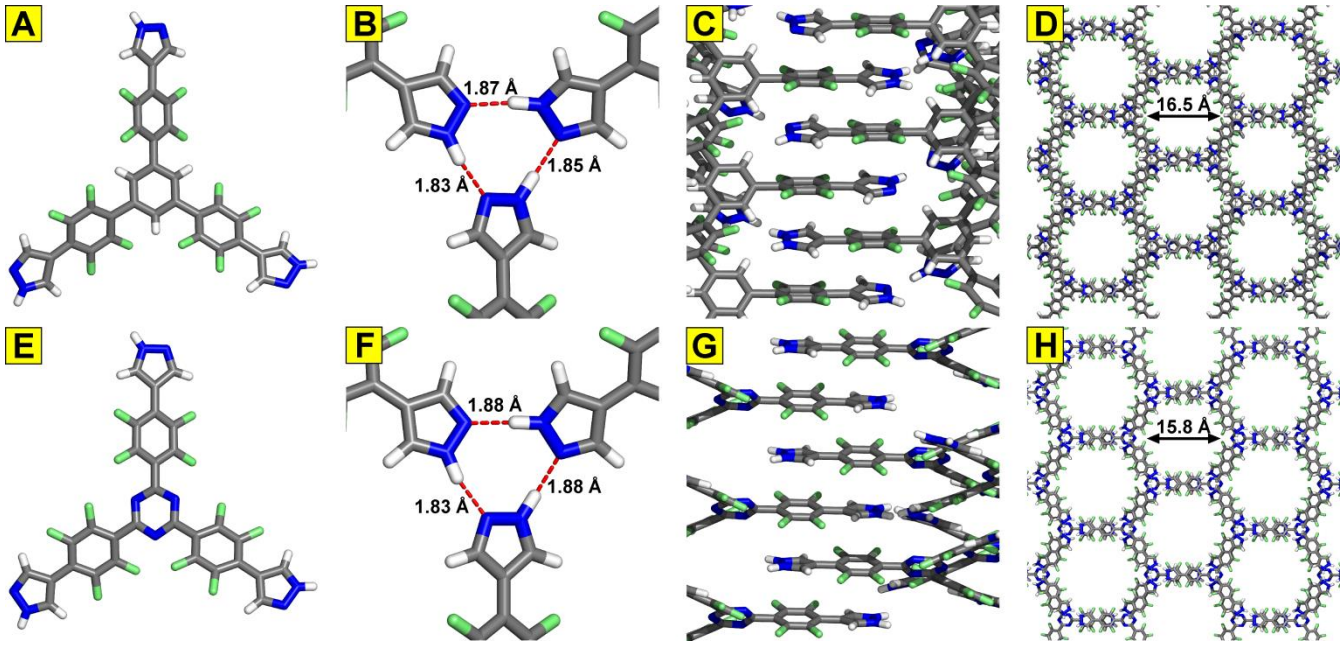

Figure 6. Crystal structures of trigonal precursors **1** (**A**) and **16** (**E**) are remarkably similar. They both form triplets of N–H···N hydrogen bonds between pyrazoles (**B** and **F**), and establish [π···π] stacking interactions between electron-rich pyrazoles and electron-poor tetrafluorobenzenes (**C** and **G**). Ultimately, both organize into porous networks with hexagonal pores (**D** and **H**).

neighboring molecules, which are parallel, offset, and separated by 3.00 Å, is much more likely caused by favorable aromatic stacking. The vertical stacks organize into parallel arrays, which are again stabilized by the offset [π···π] stacking of tetrafluorobenzenes from neighboring stacks, at a distance of 3.23 Å, as well as by the potential [C–H···π] contact between the hydrogens on the central benzene ring and the pyrazole planes (distance 2.87 Å). Overall structure defines hexagonal pores with a diameter of 11.9 Å, which are filled with partially ordered molecules of MeOH (Figure 7C). The observation of porosity in **23** suggested that the nature of the terminal hydrogen bonding group can be switched between pyrazoles and tetrazoles, and that the trimeric hydrogen bonding motif can be rotated out of plane, effectively morphing into an infinite chain of hydrogen bonds observed in **23**.

Single crystals of **26** and **27** could not be produced, but we succeeded in growing single crystals of **25**, which represents the largest crystallographically characterized compound in this study.[35] The single-crystal X-ray structure of **25** is shown in Figure 8. Three independent molecules of **25** are found in the unit cell, and two of those are connected through the disorder in their fluorinated rings; Figure 8A shows the only molecule without disorder. Relative to the plane on the central benzene ring, the three "internal" tetrafluorobenzene rings are deplanarized by 42.4–49.8 °. The twisting is highly pronounced between internal and external tetrafluorobenzene rings, with the corresponding angles in the 48.5–49.9 ° range. However, the external tetrafluorobenzenes and pyrazoles are almost coplanar, with interplanar angles in the narrow 4.5 to 12.5 ° range. Every molecule of **25** engages in the triplet of hydrogen bonds previously observed in the structures of **1**, **16**, and **19**, with [N–H···N] distances of 1.79, 1.82, and 1.88 Å (Figure 8B). The unusual structural feature of **25** is its [π···π] stacking pattern, shown in Figure 8C. Two molecules of **25** appear to have one of their arms positioned exactly on top of each other, and following that another pair of molecules oriented in the opposite direction stacks below and above them. This parallel "stacking of pairs" appears to go counter to the electron-poor/electron-rich stacking paradigm, as all of the "external" tetrafluorobenzenes appear to be stacking with each other (centroid–plane distance of 3.52 Å). Similar stacking of electron-poor aromatic rings on top of each other had been observed when two fluoroarenes were constrained by binding to the same metal cluster.[36] As the molecules from separate pairs are not parallel to each other, some of this unfavorable character may be attenuated. Half of the "internal" tetrafluorobenzenes and pyrazoles also appear to stack with each other (centroid–plane distance of 3.19 and 3.30 Å, respectively). These interactions alternate with favorable stacking of pyrazoles with "internal" tetrafluorobenzenes, characterized by the centroid–plane distance of 3.70 Å. Overall, this complex stacking pattern works together with hydrogen bonding to generate a network of hexagonal pores (Figure 8D), with a pore diameter of 26.4 Å and void volume comprising 58.1% of unit cell volume (estimated by CSD Mercury using probe radius of 1.2 Å).

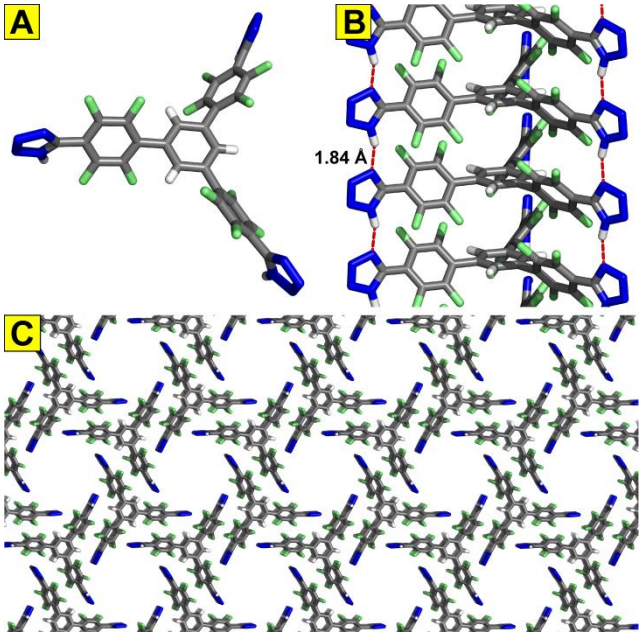

Figure 7. Crystal structure of trigonal compound **23** (**A**) shows twisting of tetrafluorobenzene rings relative to the plane of the central benzene ring. Molecules of **23** organize into vertical stacks (**B**) which are stabilized by hydrogen bonds between tetrazoles, as well as by offset [π···π] stacking of tetrafluorobenzene rings. Overall structure positions these vertical stacks parallel to each other, leaving hexagonal voids which are filled with MeOH in the as-synthesized structure (**C**, MeOH molecules removed for clarity).

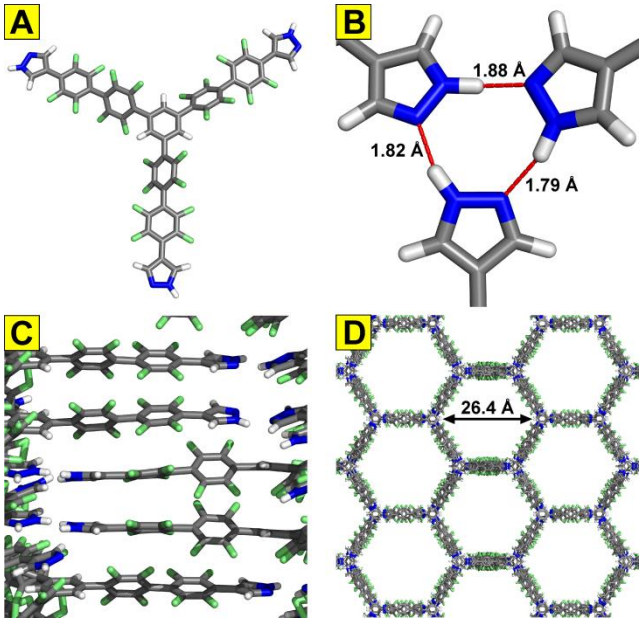

Figure 8. Crystal structure of trigonal **25** (**A**) reveals significant twisting between the central benzene ring and tetrafluorobenzenes. Triplet of [N–H···N] hydrogen bonds (**B**) and unusual pairwise [π···π] stacking (**C**) hold together the overall structure with large hexagonal channels (**D**), viewed along the crystallographic *a* axis.

Computational Analysis of Co-conformation of 25

Given the somewhat perplexing positioning of the arms of **25** above each other, we turned to computation to track the energetics of the co-conformations of dimers **25** as its arms slid past each other. To reduce computational demands, we examined a single arm of **25** through a model compound **31** (Scheme 7, top). Geometry optimization for a phenyl–perfluorophenyl–perfluorophenyl–pyrazole (Ph–Ph$_F$–Ph$_F$–Py) single-chain model was computed at B97XD/6-311+G(2d,p) level of theory, and several parallel π-stacked Ph–Ph$_F$–Ph$_F$–Py dimer models were considered at the B97D/6-31G(*d*) level. For the antiparallel π-stacked models (Scheme 7, top), the phenyl rings located at opposite end of the two chains were constrained to be co-planar, and the chain axes along the inter-ring C–C single bonds were fixed at a distance of 3.8 Å. All bond distances and bond angles were fixed to the fully optimized single-chain Ph–Ph$_F$–Ph$_F$–Py geometry, while the inter-ring dihedral angles were allowed to optimize freely. The relative energies (Δ*E*) for the various π-stacked orientations, in which the *R* distance varied from 0 Å to 14 Å in 0.4 Å increments, were computed at ωB97XD/6-311+G(d,p)//B97D/6-31G(d) level of theory and plotted against *R* in Scheme 7, bottom. At *R* = 0 Å, the phenyl (in Chain 1) and pyrazole (in Chain 2) ring centers are aligned (black dots in Scheme 7, top). Additional energy points were computed, when necessary, to capture details of the potential energy surface for parallel displacement of the π-stacked dimer model. All computations were carried out using Gaussian09.[37]

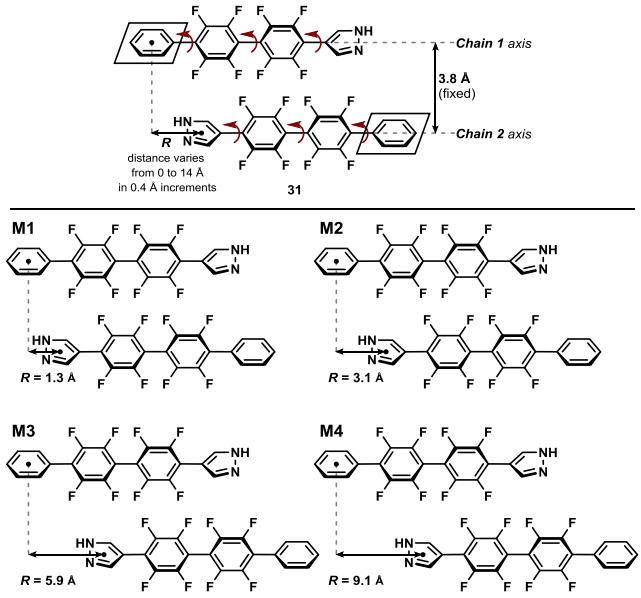

Scheme 7. Illustration of the π-stacked Ph–Ph$_F$–Ph$_F$–Py dimer of a model compound **31** (top). Red arrows illustrate the angles that were computationally allowed to vary. On the bottom, schematic illustrations of the four antiparallel π-stacked Ph–Ph$_F$–Ph$_F$–Py dimer minima **M1**–**M4** for model compound **31**.

The computed potential energy surface for parallel displacement of the π-stacked Ph–Ph$_F$–Ph$_F$–Py dimer model reveals four distinct minima structures (**M1**, **M2**, **M3**, **M4**, shown in Scheme 7, bottom) and three higher energy ridge ("peak") structures **P1**–**P3** (Figure 9). The Cartesian coordinates for **M1**–**M4** and **P1**–**P3** are included in the Supporting Information. The two lowest energy

minima, **M1** and **M2** (Scheme 7, bottom), are ~1.0 kcal mol^{-1} apart and both adopt parallel slip-stacked orientations with *R* distances of 1.3 and 3.1 Å. In particular, **M2** closely resembles the X-ray crystal structure of **25** (Figure 8C), wherein the corresponding *R* separation is 3.6 Å. The next two minima, **M3** (5.9 Å) and **M4** (9.1 Å), are 3.2 and 4.3 kcal mol^{-1} higher in energy relative to the lowest energy **M1**. In **M3**, each of the pyrazole rings is slip-stacked to the central C–C single bond between two perfluorophenyl rings (Scheme 7, bottom). In **M4**, both of the pyrazole rings are π-stacked to a perfluorophenyl ring in a "sandwich-stacked" manner (Scheme 7, bottom). These orientations minimize intermolecular F···F repulsion between the π-stacked rings; the closest F···F distances of **M1**–**M4** range from 2.77 to 3.45 Å. For comparison, the closest F···F distances for the ridge structures **P1**–**P3** are much shorter and range from 2.54 to 2.85 Å.

Calculated energy for the parallel stacking observed in the crystal structure of **25** is −7.2 kcal mol^{-1} relative to the coconformers described in Figure 9. This somewhat surprising stability is rationalized by a parallel displacement of perfluoroarene moieties of two adjacent stacks, wherein the partially negative F's of one ring are above the electron-deficient fluoroarene ring center of the other ring (distance of 3.3 Å). As a result, this arrangement benefits from some attractive electrostatic interactions.[38]

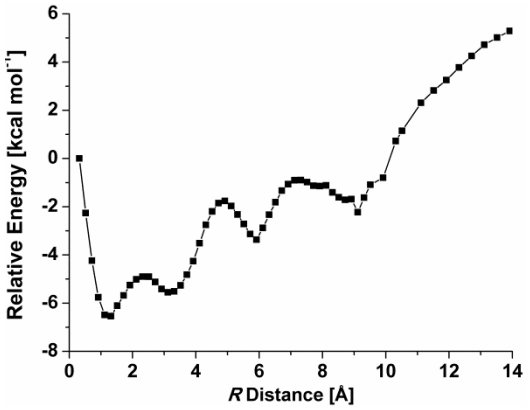

Figure 9. Computed relative energies (in kcal mol^{-1}), at the ωB97XD/6-311+G(d,p)//B97D/6-31G(d) level, for the antiparallel π-stacked Ph–Ph$_F$–Ph$_F$–Py dimers vs. the parallel displacement distance (*R*, in Å) between the centroids of the phenyl ring in Chain 1 and pyrazole ring in Chain 2.

Thermogravimetric Analysis of 16, 23, and 25

Thermogravimetric analysis (TGA, Supporting Information, Figure 72) of porous crystals of **16**, **23**, and **25** was performed in both air and N_2 in order to determine their thermal stability. Compounds **16** and **25** begin losing weight around 380 °C in both air and N_2. The weight loss of **16** in this initial stage is about 6%, and is followed by the onset of full decomposition slightly below 500 °C, as evidenced by the featureless TGA trace. This behavior is very similar to that of compound **1**.[23] Beyond 380 °C, decomposition of **25** does not have similarly distinguishable steps. Compound **23**, in contrast, appears less thermally stable, losing 16% of its weight in the well-defined first stage that begins at ~260 °C; at approx. 280 °C, featureless full decomposition begins in air and—somewhat more slowly—in N_2 as well. The initial 16% weight loss could be attributed to the loss of three (11.6%) or four (15.4%) molecules of N_2 from **23**, but the immediate onset of further decomposition prevented experimental verification of this hypothesis.

Porosity Analysis of 16, 23, and 25

Finally, gas sorption measurements were performed on **16**, **23**, and **25**, whose structures were shown to contain large pores. Nitrogen adsorption isotherm for **16** (Supporting Information, Figure 73) revealed a Brunauer-Emmett-Teller (BET) surface area of 903 m^2 g^{-1}. Using non-linear density functional theory (NLDFT) calculations the pore diameter was estimated to be ~11 Å (Supporting Information, Figure 76). This result is significantly lower than the ~18 Å pore diameter measured from the crystal structure, but existing models may not be well-suited for fluorine-lined pores such as those of **16** and **1**.[23] The surface area of **16** is smaller than that of **1** (1,159 m^2 g^{-1}), while the pore diameter appears slightly larger than measured from the crystal structure (~16 Å).

Gas sorption measurements on **23** were performed after activation by solvent exchange in *n*-pentane (4 × 24 h) and degassing of the crystals by heating at 30 °C for 24 h in vacuo. Powder X-ray diffraction patterns of the activated material were in good agreement with those simulated from single crystal data, indicating that the activation did not compromise the integrity of the samples. Compound **23** was exposed to CO_2 and N_2 at several temperatures (195, 273, and 298 K for CO_2, and 77, 195, 273, and 298 K for N_2); representative data are shown in Supporting Information, Figure 77. Adsorption of N_2 at 195 K is negligible, especially when compared to CO_2 sorption at the same. This behavior was previously observed in porous materials with nitrogen-rich functionalities.[39] From the type I adsorption isotherm observed for CO_2, Langmuir surface area of **23** was calculated to be 283 m^2 g^{-1}. At 195 K, **23** shows moderate selectivity for CO_2 versus N_2: the adsorbed quantity ratio is 14:1 in mmol g^{-1}.

Gas sorption within the pores of trigonal **25** was measured after its crystals were activated by solvent by solvent exchange in acetone (4 × 24 h) followed by *n*-pentane (4 × 24 h), and degassing of the crystals by heating at 30 °C for 24 h in vacuo. The crystal structure of trigonal **25** has several analogous characteristics with the structure of **1**, and its pore size is about 26 Å—significantly bigger than in **1** and in good agreement with NLDFT simulations (~23 Å, Supporting Information, Figure 83). As expected, the BET surface area of **25** based on nitrogen adsorption isotherm (Supporting Information, Figure 80) was determined to be 1,821 m^2 g^{-1}, which is much higher than in **1**.

The measured surface areas match quite well with the calculated values obtained from crystal structure data using Materials Studio software package. These calculated surface areas are 1,447 m^2 g^{-1} for **1**, 1,371 m^2 g^{-1} for **16**, 667 m^2 g^{-1} for **23**, and 1,598 m^2 g^{-1} for **25**.

CONCLUSIONS

In summary, we have performed one of the most comprehensive examinations of structure/porosity relationships among porous molecular crystals. More than a dozen potential precursors to porous molecular all-organic crystals were synthesized using a

combination of Cu and Pd catalysis, protecting group chemistry on the nitrogen, and solvothermal synthesis. Within the series, geometry, length, and the propensity for hydrogen bonding and [π···π] stacking were varied. Crystal structures of analyzed precursors reveal that hydrogen bonding and [π···π] stacking capabilities are both required for the formation of a porous structure. Among all the analyzed precursors, only the trigonal ones showed porous structures, suggesting that this geometry is required as well.[40] Within this set of restrictions, some modifications are allowed. Hydrogen bonding group can be changed from a pyrazole (in **1**) to a tetrazole (in **23**). This change shifts the hydrogen bonding pattern from being in a plane perpendicular to the one dimensional pores, to running in a direction that is parallel to these 1D pores. The nature of the central ring can be changed from a 1,3,5-substituted benzene (in **1**) to a 1,3,5-triazene (in **16**); the two derivatives are essentially isostructural but demonstrate important differences in solution-phase emission. Finally, and perhaps most significantly, the length of the three arms of **1** can be extended by an insertion of another 1,2,4,5-tetrafluorinated benzene ring, resulting in geometrically larger pores in **25**. Overall, three new porous structures were identified; their surface areas are moderate. The observed variations within this series of related compounds also contribute to the ongoing efforts to predict porosity in discrete molecules.[41]

Future work in our labs will explore (*a*) incorporation of some of the prepared pyrazole ligands into MOFs, similar to the previously reported reticulation of **23** into a fluorinated MOF;[27a] (*b*) behavior of these frameworks under pressure, and (*c*) the effects of switching the tetrafluorobenzene group to other electron-poor connectors. Results of these studies will be reported in due course.

ASSOCIATED CONTENT

Supporting Information. Synthetic procedures and full characterization data for all new compounds, Cartesian coordinates for co-conformers of $\mathbf{31}_2$, crystal structures of **4**, **6**, **19**, and **20**, gas sorption and TGA data. This material is available free of charge via the Internet at http://pubs.acs.org.

AUTHOR INFORMATION

Corresponding Author

*miljanic@uh.edu

Present Addresses

Teng-Hao Chen, Department of Chemistry, Tamkang University, No. 151 Yingzhuan Rd., Tamsui District, New Taipei City 25137, TAIWAN.

Watchareeya Kaveevivitchai, Department of Chemical Engineering, National Cheng Kung University, No. 1 University Rd., East District, Tainan City 70101, TAIWAN.

Ilja Popovs, Chemical Science Division, Oak Ridge National Laboratory, Oak Ridge, TN 37831, USA.

ACKNOWLEDGMENT

We acknowledge the financial support from the University of Houston and its Grant to Advance and Enhance Research (to O. Š. M.), the National Science Foundation (award DMR-1507664 to O. Š. M. and O. D.), and the Welch Foundation (awards E-0024 to A.J.J. and E-1768 to O. Š. M., c hair E-0044 to O. D.). O. Š. M. is a Cottrell Scholar of the Research Corporation for Science Advancement. ChemMatCARS Sector 15 is principally supported by the National Science Foundation under grant number CHE-1346572. Use of the Advanced Photon Source was supported by the U. S. Department of Energy, Office of Science, Office of Basic Energy Sciences, under Contract No. DE-AC02-06CH11357.

REFERENCE

(1) (*a*) Schüth, F.; Sing, K. S. W.; Weitkamp, J. *Handbook of Porous Solids*, John Wiley & Sons: Hoboken, NJ, **2002**. (*b*) Slater, A. G.; Cooper, A. I. *Science* **2015**, *348*, 988.

(2) (*a*) *Metal-Organic Frameworks: Applications from Catalysis to Gas Storage*, Farrusseng, D. (Ed.); Wiley-VCH: Weinheim, **2011**. (*b*) *Metal-Organic Frameworks: Design and Application*, MacGillivray, L. R. (Ed.); Wiley: Hoboken, **2010**. (*c*) Special issue of *Chem. Rev.* **2012**, *112*, 673–1268. (*d*) Special issue of *Chem. Soc. Rev.* **2009**, *38*, 1201–1508.

(3) (*a*) Huang, N.; Wang, P.; Jiang, D. *Nat. Rev. Mater.* **2016**, *1*, doi:10.1038/natrevmats.2016.68. (*b*) Ding, S.-Y.; Wang, W. *Chem. Soc. Rev.* **2013**, *42*, 548–568. (*c*) Côté, A. P.; Benin, A. I.; Ockwig, N.W.; O'Keeffe, M.; Matzger, A. J.; Yaghi, O. M. *Science* **2005**, *310*, 1166–1170.

(4) For an example of a porous amorphous organic polymer, see: Jiang, J.-X.; Su, F.; Trewin, A.; Wood, C. D.; Campbell, N. L.; Niu, H.; Dickinson, C.; Ganin, A. Y.; Rosseinsky, M. J.; Khimyak, Y. Z.; Cooper, A. I. *Angew. Chem. Int. Ed.* **2007**, *46*, 8574–8578.

(5) Significant recent advances, however, have been made in the preparation of thin films and membranes from MOFs and COFs. See: (*a*) Shekhah, O.; Liu, J.; Fischer, R. A.; Wöll, Ch. *Chem. Soc. Rev.* **2011**, *40*, 1081–1106. (*b*) Qiu, S.; Xue, M.; Zhu, G. *Chem. Soc. Rev.* **2014**, *43*, 6116–6140. (*c*) Bisbey, R. P.; DeBlase, C. R.; Smith, B. J.; Dichtel, W. R. *J. Am. Chem. Soc.* **2016**, *138*, 11433–11436. (*d*) Colson, J. W.; Woll, A. R.; Mukherjee, A.; Levendorf, M. P.; Spitler, E. L.; Shields, V. B.; Spencer, M. G.; Park, Y.; Dichtel, W. R. *Science* **2011**, *332*, 228–231.

(6) For reviews, see: (*a*) Cooper, A. I. *Acs Cent. Sci.* **2017**, *3*, 544–553. (*b*) Hasell, T.; Cooper, A. I. *Nat. Rev. Mater.* **2016**, *1*, doi:10.1038/natrevmats.2016.53. (*c*) Hashim, M. I.; Hsu, C.-W.; Le, H. T. M.; Miljanić, O. Š. *Synlett* **2016**, *27*, 1907–1918. (*d*) Evans, J. D.; Sumby, C. J.; Doonan, C. J. *Chem. Lett.* **2015**, *44*, 582–588. (*e*) Zhang, G.; Mastalerz, M. *Chem. Soc. Rev.* **2014**, *43*, 1934–1947. (*f*) Mastalerz, M. *Synlett* **2013**, *24*, 781–786. (*g*) Tian, J.; Thallapally, P. K.; McGrail, B. P. *CrystEngComm* **2012**, *14*, 1909–1919. (*h*) Holst, J. R.; Trewin, A.; Cooper, A. I. *Nat. Chem.* **2010**, *2*, 915–920. (*i*) McKeown, N. B. *J. Mater. Chem.* **2010**, *20*, 10588–10597. (*j*) Barbour, L. J. *Chem. Commun.* **2006**, 1163–1168.

(7) (*a*) Zhang, G.; Presly, O.; White, F.; Oppel, I. M.; Mastalerz, M. *Angew. Chem. Int. Ed.* **2014**, *53*, 5126–5130. (*b*) Zhang, G.; Presly, O.; White, F.; Oppel, I. M.; Mastalerz, M. *Angew. Chem. Int. Ed.* **2014**, *53*, 1516–1520. See also: (c) Ono, K.; Johmoto, K.; Yasuda, N.; Uekusa, H.; Fujii, S.; Kiguchi, M.; Iwasawa, N. *J. Am. Chem. Soc.* **2015**, *137*, 7015–7018.

(8)(*a*) Elbert, S. M.; Rominger, F.; Mastalerz, M. *Chem. Eur. J.* **2014**, *20*, 16707–16720. (*b*) Schneider, M. W.; Oppel, I. M.; Ott, H.; Lechner, L. G.; Hauswald, H.-J. S.; Stoll, R.; Mastalerz, M. *Chem. Eur. J.* **2012**, *18*, 836–847. (*c*) Jones, J. T. A.; Hasell, T.; Wu, X.; Bacsa, J.; Jelfs, K. E.; Schmidtmann, M.; Chong, S. Y.; Adams, D. J.; Trewin, A.; Schiffman, F.; Cora, F.; Slater, B.; Steiner, A. ; Day, G. M.; Cooper, A. I. *Nature* **2011**, *474*, 367–371. (*d*) Bojdys, M. J.; Briggs, M. E.; Jones, J. T. A.; Adams, D. J.; Chong, S. Y.; Schmidtmann, M.; Cooper, A. I. *J. Am. Chem. Soc.* **2011**, *113*, 16566–16571. (*e*) Mastalerz, M.; Schneider, M. W.; Oppel, I. M.; Presly, O. *Angew. Chem. Int. Ed.* **2011**, *50*, 1046–1051. (*f*) Tozawa, T.; Jones, J. T. A.; Swamy, S. I.; Jiang, S.; Adams, D. J.; Shakespeare, S.; Clowes, R.; Bradshaw, D.;. Hasell, T.; Chong, S. Y.; Tang, C.; Thompson, S.; Parker, J.; Trewin,

A.; Bacsa, J.; Slawin, A. M. Z.; Steiner, A.; Cooper, A. I. *Nat. Mater.* **2009**, *8*, 973–978. (*g*) Mastalerz, M. *Chem. Commun.* **2008**, 4756–4758.

(9) (*a*) Burgun, A.; Valente, P.; Evans, J. D.; Huang, D. M.; Sumby, C. J.; Doonan, C. J. *Chem. Commun.* **2016**, *52*, 8850–8853. (*b*) Evans, J. D.; Huang, D. M.; Hill, M. R.; Sumby, C. J.; Sholl, D. S.; Thornton, A. W.; Doonan, C. J. *J. Phys. Chem. C* **2015**, *119*, 7746–7754. (*c*) Avellaneda, A.; Valente, P.; Burgun, A.; Evans, J. D.; Markwell-Heys, A. W.; Rankine, D.; Nielsen, D. J.; Hill, M. R.; Sumby, C. J.; Doonan, C. J. *Angew. Chem. Int. Ed.* **2013**, *52*, 3746–3749.

(10) (*a*) Ji, Q.; Le, H. T. M.; Wang, X.; Chen, Y.-S.; Makarenko, T.; Jacobson, A. J.; Miljanić, O. Š. *Chem. Eur. J.* **2015**, *21*, 17205–17209. See also: (*b*) Ji, Q.; Do, L. H.; Miljanić, O. Š. *Synlett* **2015**, *26*, 1625–1627.

(11)(*a*) Kohl, B.; Rominger, F.; Mastalerz, M. *Chem. Eur. J.* **2015**, *21*, 17308–17313. (*b*) Kohl, B.; Rominger, F.; Mastalerz, M. *Org. Lett.* **2014**, *16*, 704–707. (*c*) Mastalerz, M.; Oppel, I. M. *Angew. Chem. Int. Ed.* **2012**, *51*, 5252–5255.

(12) Beaudoin, D.; Rominger, F.; Mastalerz, M. *Angew. Chem. Int. Ed.* **2016**, *55*, 15599–15603.

(13) (*a*) Wang, H.; Li, B.; Wu, H.; Hu, T.-L.; Yao, Z.; Zhou, W.; Xiang, S.; Chen, B. *J. Am. Chem. Soc.* **2015**, *137*, 9963–9970. (*b*) Yang, W.; Li, B.; Wang, H.; Alduhaish, O.; Alfooty, K.; Zayed, M. A.; Li, P.; Arman, H. D.; Chen, B. *Cryst. Growth Des.* **2015**, *15*, 2000–2004. (*c*) Li, P.; He, Y.; Zhao, Y.; Weng, L.; Wang, H.; Krishna, R.; Wu, H.; Zhou, W.; O'Keeffe, M.; Han, Y.; Chen, B. *Angew. Chem. Int. Ed.* **2015**, *54*, 574–577. (*d*) Li, P.; He, Y.; Arman, H. D.; Krishna R.; Wang, H.; Weng, L. and Chen, B. *Chem. Commun.* **2014**, 50, 13081–13084. (*e*) Li, P.; He, Y.; Guang, J.; Weng, L.; Zhao, J. C.-G.; Xiang, S.; Chen, B. *J. Am. Chem. Soc.* **2014**, *136*, 547–549. (*f*) He, Y.; Xiang, S.; Chen, B. *J. Am. Chem. Soc.* **2011**, *133*, 14570–14573.

(14) (*a*) Brunet, P.; Simard, M.; Wuest, J. D. *J. Am. Chem. Soc.* **1997**, *119*, 2737–2738. (*b*) Malek, N.; Maris, T.; Simard, M.; Wuest, J. D. *J. Am. Chem. Soc.* **2005**, *127*, 5910–5916.

(15) Wu, Y.-L.; Horwitz, N. E.; Chen, K.-S.; Gomez-Gualdron, D. A.; Luu, N. S.; Ma, L.; Wang, T. C.; Hersam, M. C.; Hupp, J. T.; Farha, O. K.; Snurr, R. Q.; Wasielewski, M. R. *Nat. Chem.* **2017**, *9*, 466–472.

(16) (*a*) Song, Q.; Jiang, S.; Hasell, T.; Liu, M.; Sun, S.; Cheetham, A. K.; Sivaniah, E.; Cooper, A. I. *Adv. Mater.* **2016**, *28*, 2629–2637. (*b*) Bushell, A. F.; Budd, P. M.; Attfield, M. P.; Jones, J. T. A.; Hasell, T.; Cooper, A. I.; Bernardo, P.; Bazzarelli, F.; Clarizia, G.; Jansen, J. C. *Angew. Chem. Int. Ed.* **2012**, *52*, 1253–1256.

(17) Liu, M.; Chen, L.; Lewis, S.; Chong, S. Y.; Little, M. A.; Hasell, T.; Aldous, I. M.; Brown, C. M.; Smith, M. W.; Morrison, C. A.; Hardwick, L. J.; Cooper, A. I. *Nat. Commun.* **2016**, *7*, doi:10.1038/ncomms12750.

(18) Chen, L.; Reiss, P. S.; Chong, S. Y.; Holden, D.; Jelfs, K. E.; Hasell, T.; Little, M. A.; Kewley, A.; Briggs, M. E.; Stephenson, A.; Thomas, K. M.; Armstrong, J. A.; Bell, J.; Busto, J.; Noel, R.; Liu, J.; Strachan, D. M.; Thallapally, P. K.; Cooper, A. I. *Nat. Mater.* **2014**, *13*, 954–960.

(19) Jones, J. T. A.; Holden, D.; Mitra, T.; Hassel, T.; Adams, D. J.; Jelfs, K. E.; Trewin, A.; Willock, D. J.; Day, G. M.; Bacsa, J.; Steiner, A.; Cooper, A. I. *Angew. Chem. Int. Ed.* **2011**, *50*, 749–753.

(20) (*a*) Brutschy, M.; Schneider, M. W.; Mastalerz, M.; Waldvogel, S. R. *Chem. Commun.* **2013**, *49*, 8398–8400. (*b*) Brutschy, M.; Schneider, M. W.; Mastalerz, M.; Waldvogel, S. R. *Adv. Mater.* **2012**, *24*, 6049–6052.

(21) (*a*) Giri, N.; del Pópolo, M. G.; Melaugh, G.; Greenaway, R. L.; Rätzke, K.; Koschine, T.; Pison, L.; Costa Gomes, M. F.; Cooper, A. I.; James, S. L. *Nature* **2015**, *527*, 216–220. (*b*) Zhang, J.; Chai, S.-H.; Qiao, Z.-A.; Mahurin, S. M.; Chen, J.; Fang, Y.; Wan, S.; Nelson, K.; Zhang, P.; Dai, S. *Angew. Chem. Int. Ed.* **2015**, *54*, 932–936.

(22) Hasell, T.; Chong, S. Y.; Schmidtmann, M.; Adams, D. J.; Cooper, A. I. *Angew. Chem. Int. Ed.* **2012**, *51*, 7154–7157.

(23) Chen, T.-H.; Popov, I.; Kaveevivitchai, W.; Chuang, Y.-C.; Chen, Y.-S.; Daugulis, O.; Jacobson, A. J.; Miljanić, O. Š. *Nat. Commun.* **2014**, *5*, doi: 10.1038/ncomms6131.

(24) (*a*) Boldog, I.; Rusanov, E. B.; Sieler, J.; Blaurock, S.; Domasevitch, K. V. *Chem. Commun* **2003**, 740–741. (*b*) Alkorta, I.; Elguero, J.; Foces-Foces, C.; Infantes, L. *ARKIVOC* **2006**, 15–30.

(25) Chen, T.-H.; Kaveevivitchai, W.; Jacobson, A. J.; Miljanić, O. Š. *Chem. Comm.* **2015**, *51*, 14096–14098.

(26) Hendon, C. H.; Wittering, K. E.; Chen, T.- H.; Kaveevivitchai, W.; Popov, I.; Butler, K. T.; Wilson, C. C.; Cruickshank, D. L.; Miljanić, O. Š.; Walsh, A. *Nano Lett.* **2015**, *15*, 2149–2154.

(27) (*a*) Chen, T.-H.; Popov, I.; Kaveevivitchai, W.; Chuang, Y.-C.; Chen, Y.-S.; Jacobson, A. J.; Miljanić, O. Š. *Angew. Chem. Int. Ed.* **2015**, *54*, 13902–13906. (*b*) Chen, T.-H.; Popov, I.; Zenasni, O.; Daugulis, O.; Miljanić, O. Š. *Chem. Commun.* **2013**, *49*, 6846–6848.

(28) For the synthesis of nonfluorinated analogs of **1**–**3**, see: (*a*) Kershaw Cook, L. J.; Kearsey, R.; Lamb, J. V.; Pace, E. J.; Gould, J. A. *Tetrahedron Lett.* **2016**, *57*, 895–898. For crystal structure of nonfluorinated analog of **2**, see: (*b*) Maspero, A.; Galli, S.; Masciocchi, N.; Palmisano, G. *Chem. Lett.* **2008**, *37*, 956–957. For For crystal structure of nonfluorinated analog of **3**, see: (*c*) Masciocchi, N.; Galli, S.; Colombo, V.; Maspero, A.; Palmisano, G.; Seyyedi, B.; Lamberti, C.; Bordiga, S. *J. Am. Chem. Soc.* **2010**, *132*, 7902– 7904.

(29) Elguero, J.; Jaramillo, C.; Pardo, C. *Synthesis* **1997**, *1997*, 563–566.

(30) (*a*) Deshpande, R. K.; Minnaar, J. L.; Telfer, S. G. *Angew. Chem. Int. Ed.* **2010**, *49*, 4598–4602. For procedures that proceed to bind the ligands liberated after the solvothermal cleavage of the Boc group to a metal, see: (*b*) Procopio, E. Q.; Padial, N. M.; Masciocchi, N.; Galli, S.; Oltra, J. E.; Barea, E.; Navarro, J. A. R. *CrystEngComm.* **2013**, *15*, 9352–9355. (*c*) Padial, N. M.; Procopio, E. Q.; Montoro, C.; López, E.; Oltra, J. E.; Colombo, V.; Maspero, A.; Masciocchi, N.; Galli, S.; Senkovska, I.; Kaskel, S.; Barea, E.; Navarro, J. A. R. *Angew. Chem. Int. Ed.* **2013**, *52*, 8290–8294.

(31) Miller, A. O.; Krasnov, V. I.; Peters, D.; Platonov, V. E.; Miethchen, R. *Tetrahedron Lett.* **2000**, *41*, 3817–3819.

(32) Zhang, Z.; Hashim, M. I.; Miljanić, O. Š. *Chem. Commun.* **2017**, *53*, 10022–10025.

(33) In all structures, N–H and C–H bond lengths have been normalized to values obtained from neutron diffraction measurements. See: Steiner, T. *Angew. Chem. Int. Ed.* **2002**, *41*, 48–76.

(34) The formation of infinite catemers in the solid-state structures of **2** and **4**, and their absence in the case of **3**, could be tentatively rationalized by the coplanar arrangement of two terminal pyrazoles in **2** and **4**, and their deplanarization in **3**. In analogous rigid dicarboxylic acids, both forms are observed, suggesting small energy differences between the two forms. See: (*a*) Beyer, T.; Price, S. L. *J. Phys. Chem. B*, **2000**, *104*, 2647–2655. In fact, there are examples of rigid dicarboxylic acids wherein the coplanarity of the –COOH groups leads to the formation of dimers, exactly the opposite from our observation for pyrazoles. See: (*b*) Dang, H.; Maris, T.; Yi, J.-H.; Rosei, F.; Nanci, A.; Wuest, J. D. *Langmuir* **2007**, *23*, 11980–11985.

(35) Disordered solvent found in the pores of **25** was excluded from the analysis using PLATON/SQUEEZE routine. A total of 15,333 electrons were treated in this manner, corresponding to 11.98 molecules of DMF per molecule of **25** (with the assumption that DMF was the only guest found in the pores).

(36) See, for example: (*a*) Bosch, E.; Bowling, N. P.; Darko, J. *Cryst. Growth Des.* **2015**, *15*, 1634–1641. (*b*) Bojan, R. V.; Czerwieniec, R.; Laguna, A.; Lasanta, T.; López-de-Luzuriaga, J. M.; Monge, M.; Olmos, M. E.; Yersin, H. *Dalton Trans.* **2013**, *42*, 4267–4277. (*c*) Cotton, F. A.; Lin, C.; Murillo, C. A. *Inorg. Chem.* **2001**, *40*, 5886–5889. (*d*) Goodhand, N.; Hamor, T. A. *Acta Cryst.* **1982**, *B38*, 1342–1345.

(37) Gaussian 09, Frisch, M. J.; Trucks, G. W.; Schlegel, H. B.; Scuseria, G. E.; Robb, M. A.; Cheeseman, J. R.; Scalmani, G.; Barone, V.; Petersson, G. A.; Nakatsuji, H.; Li, X.; Caricato, M.; Marenich, A.; Bloino, J.; Janesko, B. G.; Gomperts, R.; Mennucci, B.; Hratchian, H. P.; Ortiz, J. V.; Izmaylov, A. F.; Sonnenberg, J. L.; Williams-Young, D.; Ding, F.; Lipparini, F.; Egidi, F.; Goings, J.; Peng, B.; Petrone, A.; Henderson, T.; Ranasinghe, D.; Zakrzewski, V. G.; Gao, J.; Rega, N.; Zheng, G.; Liang, W.; Hada, M.; Ehara, M.; Toyota, K.; Fukuda, R.; Hasegawa, J.; Ishida, M.; Nakajima, T.; Honda, Y.; Kitao, O.; Nakai, H.; Vreven, T.; Throssell, K.; Montgomery, J. A. Jr.; Peralta, J. E.; Ogliaro, F.; Bearpark, M.; Heyd, J. J.; Brothers, E.; Kudin, K. N.; Staroverov, V. N.; Keith, T.; Kobayashi, R.; Normand, J.; Raghavachari, K.; Rendell, A.; Burant, J. C.; Iyengar, S. S.; Tomasi, J.; Cossi, M.; Millam, J. M.; Klene, M.; Adamo, C.; Cammi, R.; Ochterski, J. W.; Martin, R. L.; Morokuma, K.; Farkas, O.; Foresman, J. B.; Fox, D. J. Gaussian, Inc., Wallingford CT, 2016.

(38) Wheeler, S. E. *Acc. Chem. Res.* **2013**, *46*, 1029–1038.

(39) Patel, H. A.; Je, S. H.; Park, J.; Chen, D. P.; Jung, Y.; Yavuz, C. T.; Coskun, A. *Nat. Commun.* **2013**, *4*, doi:10.1038/ncomms2359.

(40) However, some geometries that have not been examined could prove to lead to other porous structures. An example would be the tetragonal geometry based on 1,2,4,5-tetrasubstituted benzene as the central core.

(41) (*a*) Garcia, I. G.; Bernabei, M.; Soto, R. P.; Haranczyk, M. *Cryst. Growth Des.* **2017**, *17*, 5614–5619. (*b*) Evans, J. D.; Huang, D. M.; Haranczyk, M.; Thornton, A. W.; Sumby, C. J.; Doonan, C. J. *CrystEngComm* **2016**, *18*, 4133– 4141.

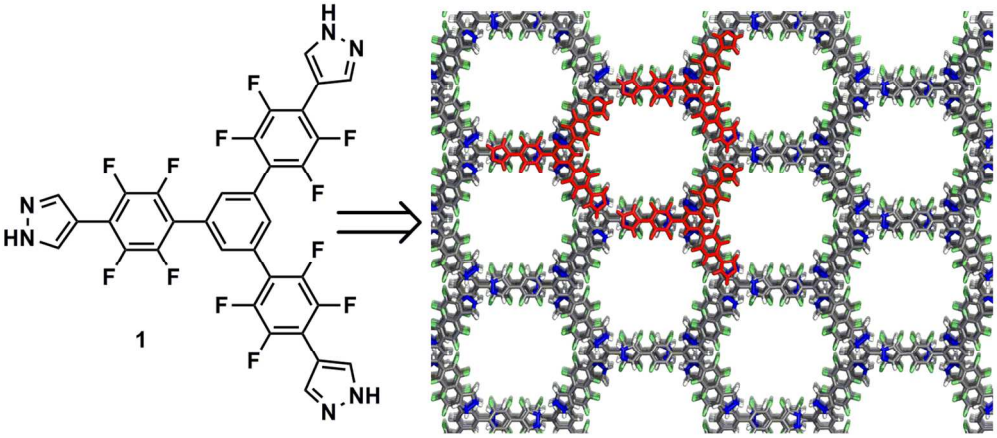

124x55mm (300 x 300 DPI)

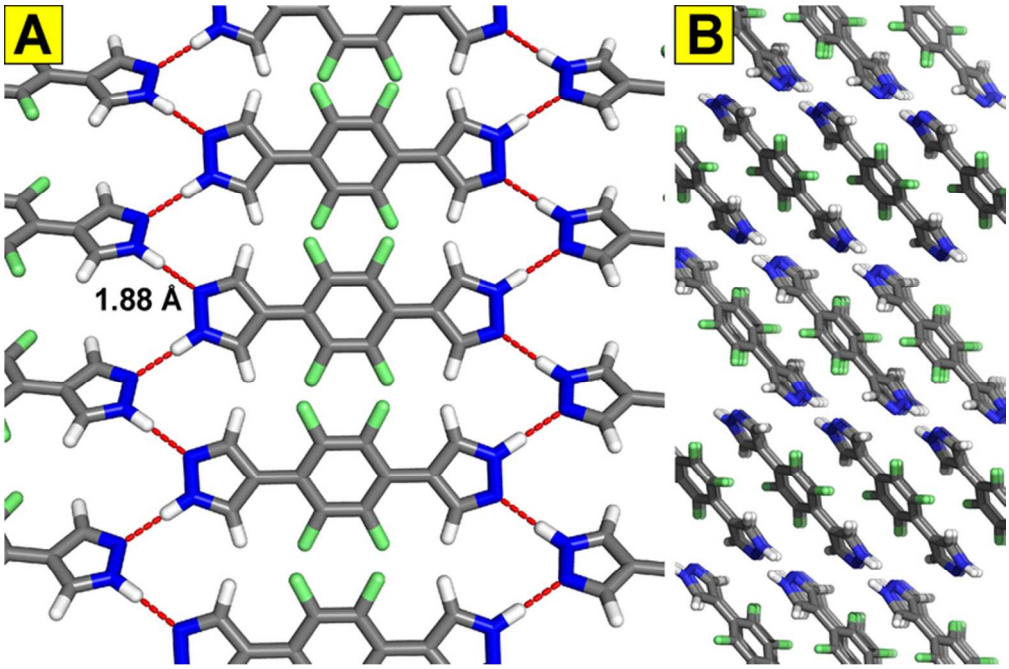

66x44mm (300 x 300 DPI)

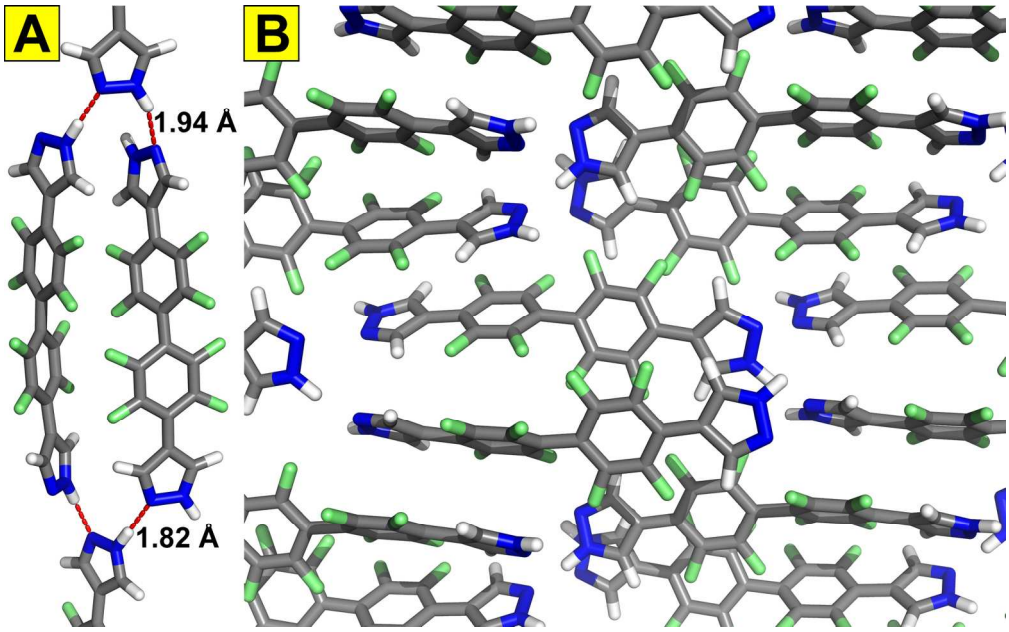

169x105mm (300 x 300 DPI)

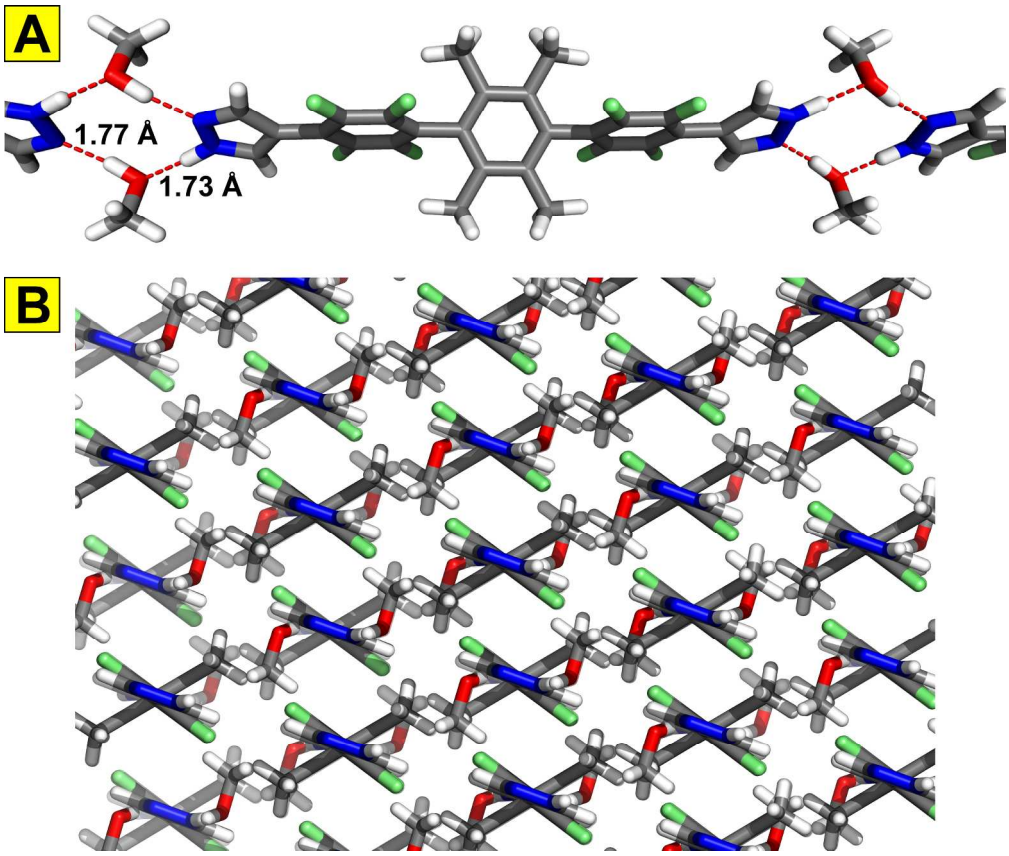

229x193mm (300 x 300 DPI)

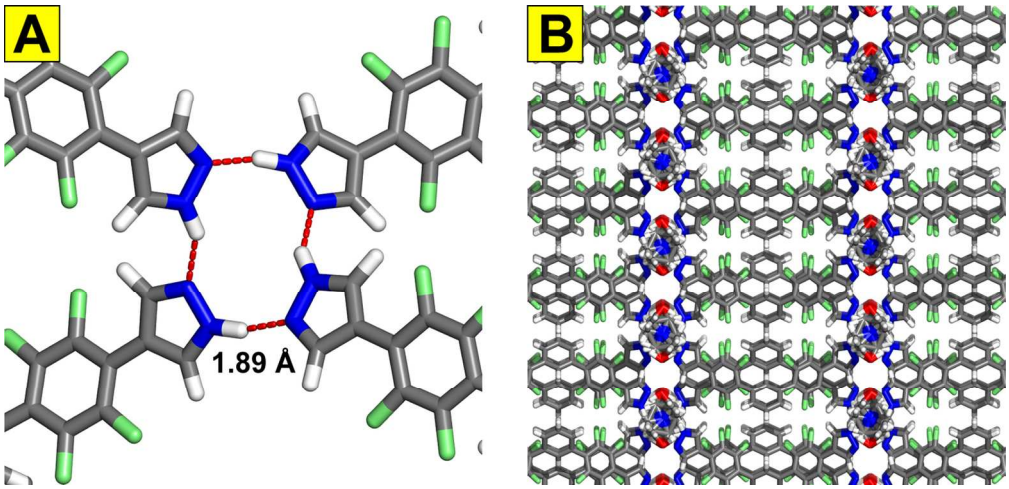

129x61mm (300 x 300 DPI)

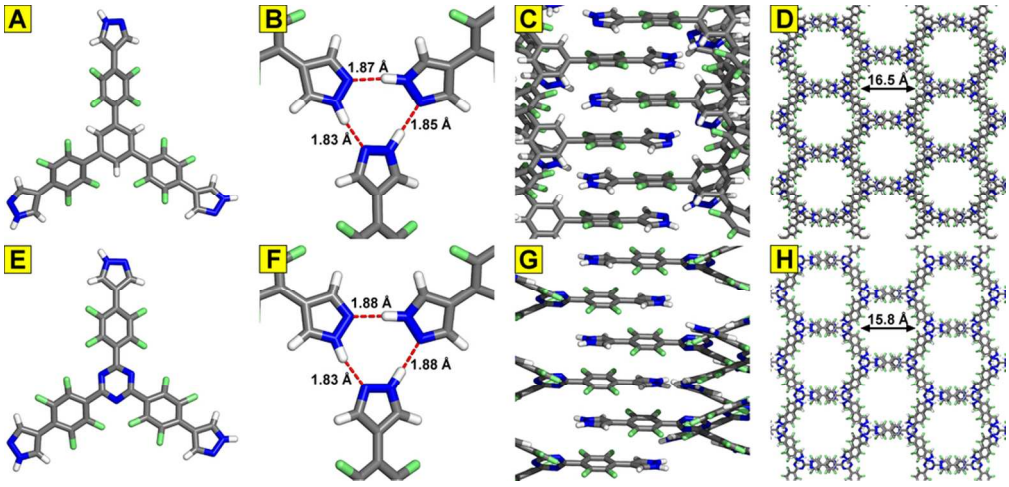

95x45mm (300 x 300 DPI)

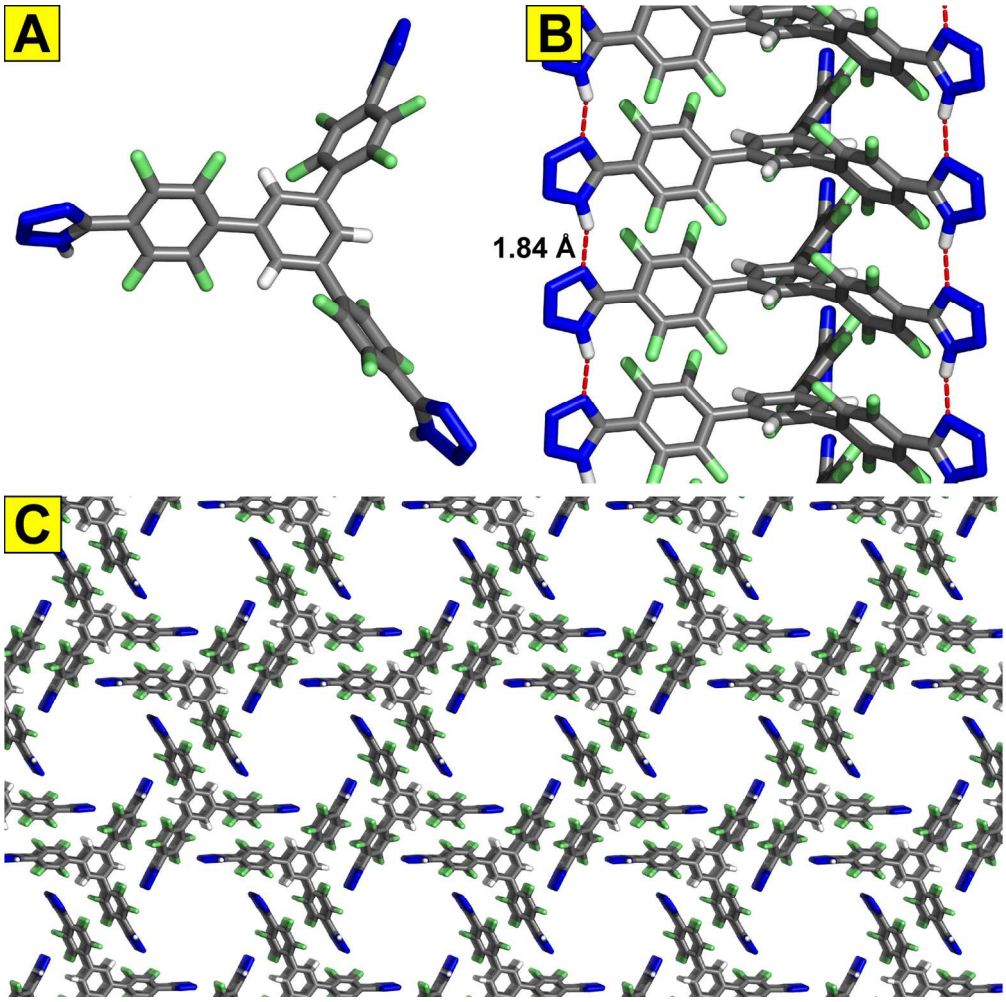

148x146mm (300 x 300 DPI)

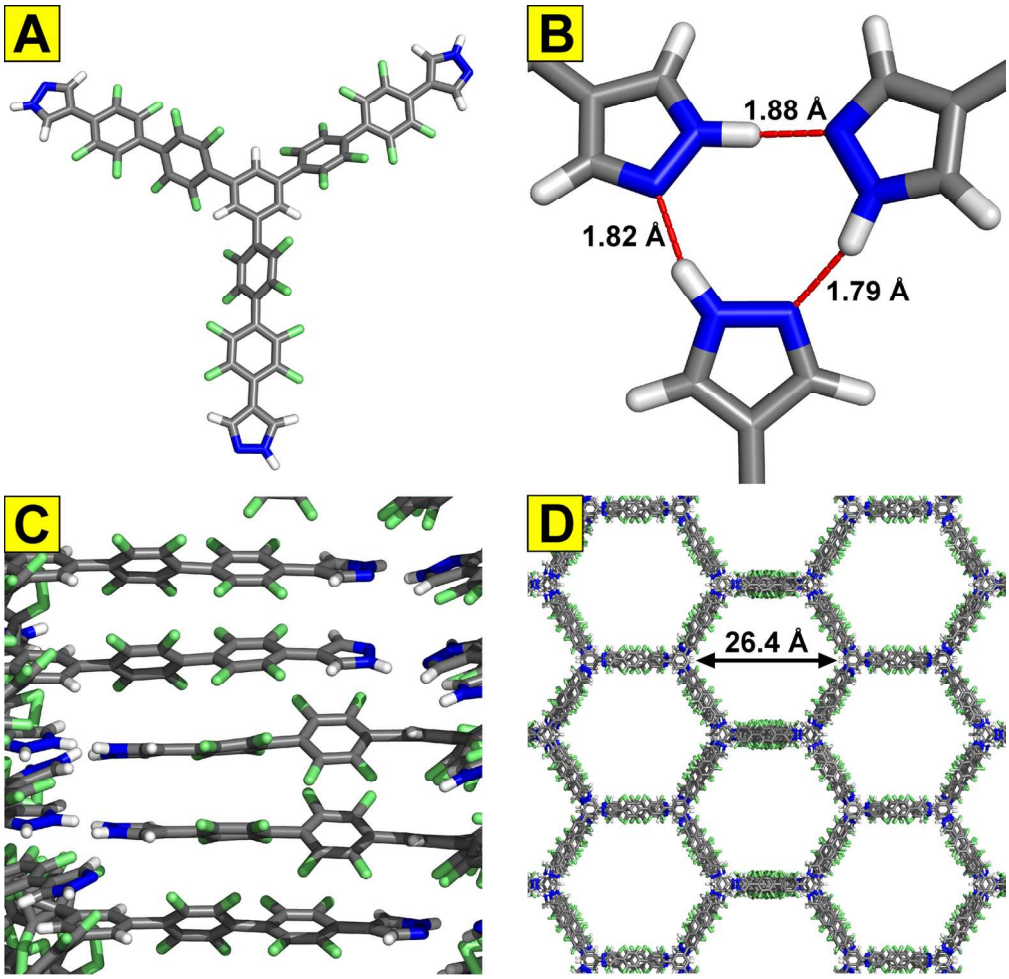

145x140mm (300 x 300 DPI)

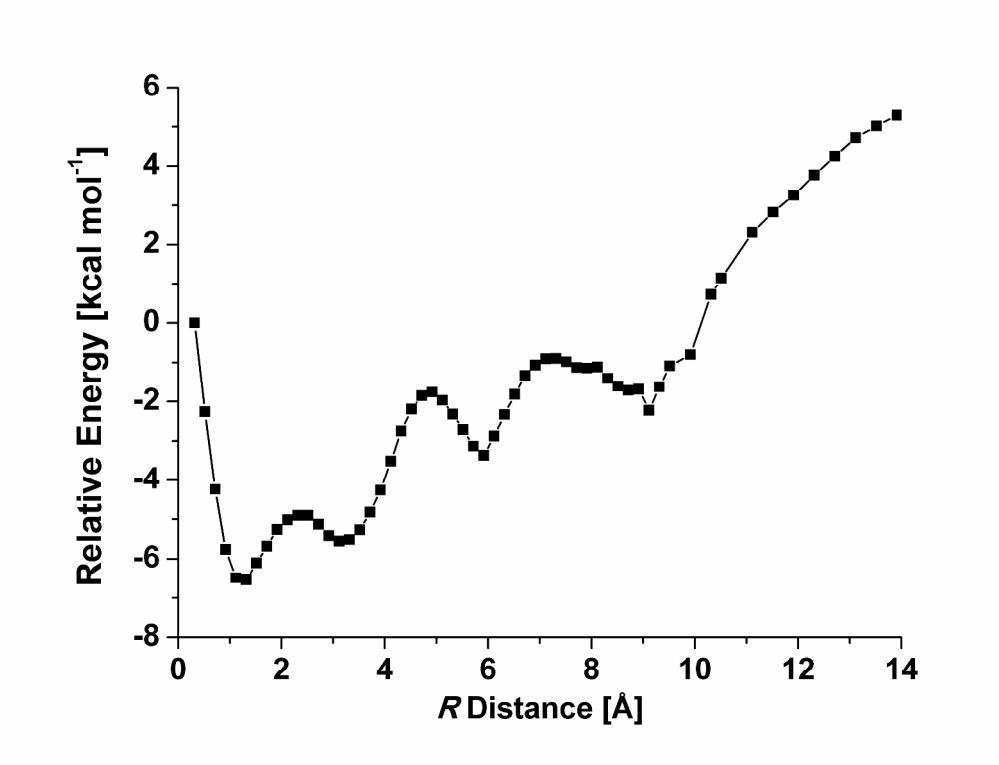

423x324mm (300 x 300 DPI)

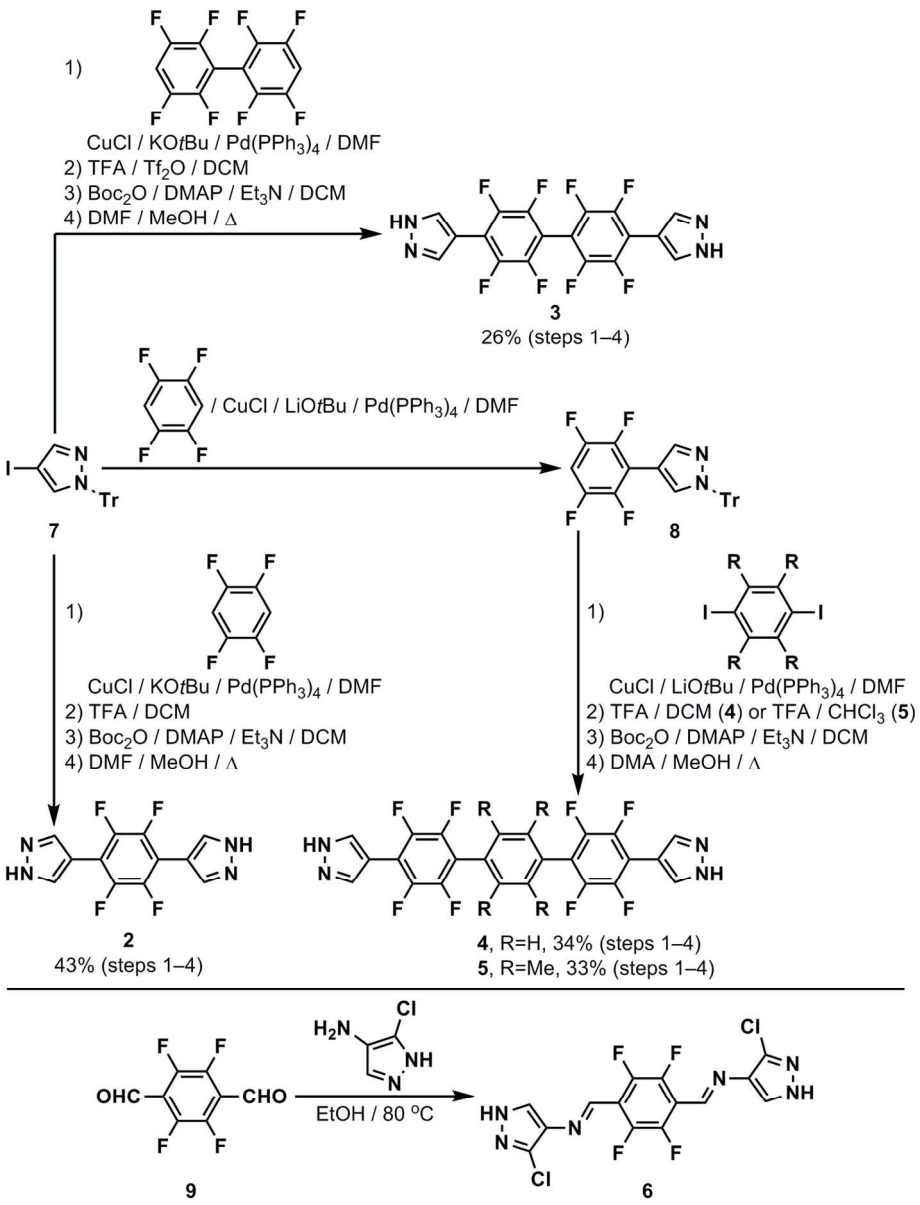

127x166mm (300 x 300 DPI)

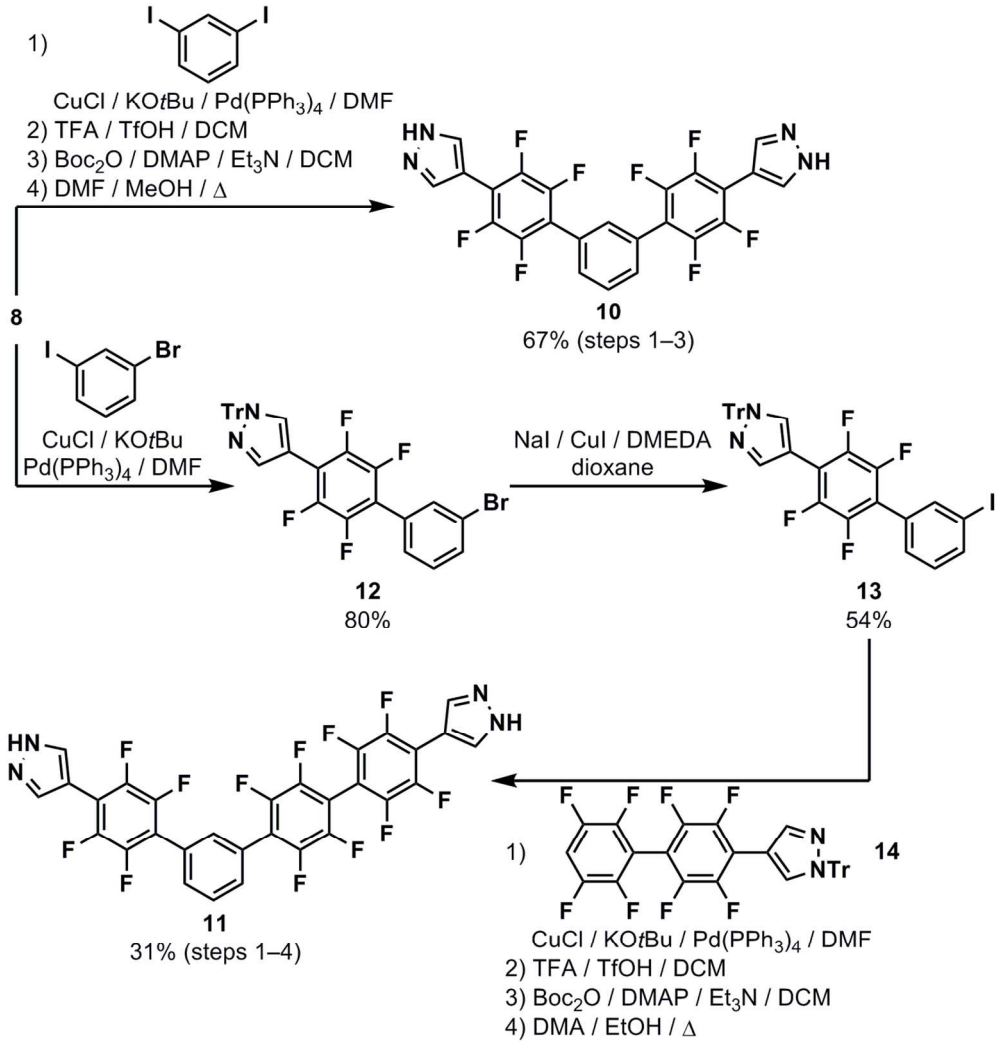

119x125mm (300 x 300 DPI)

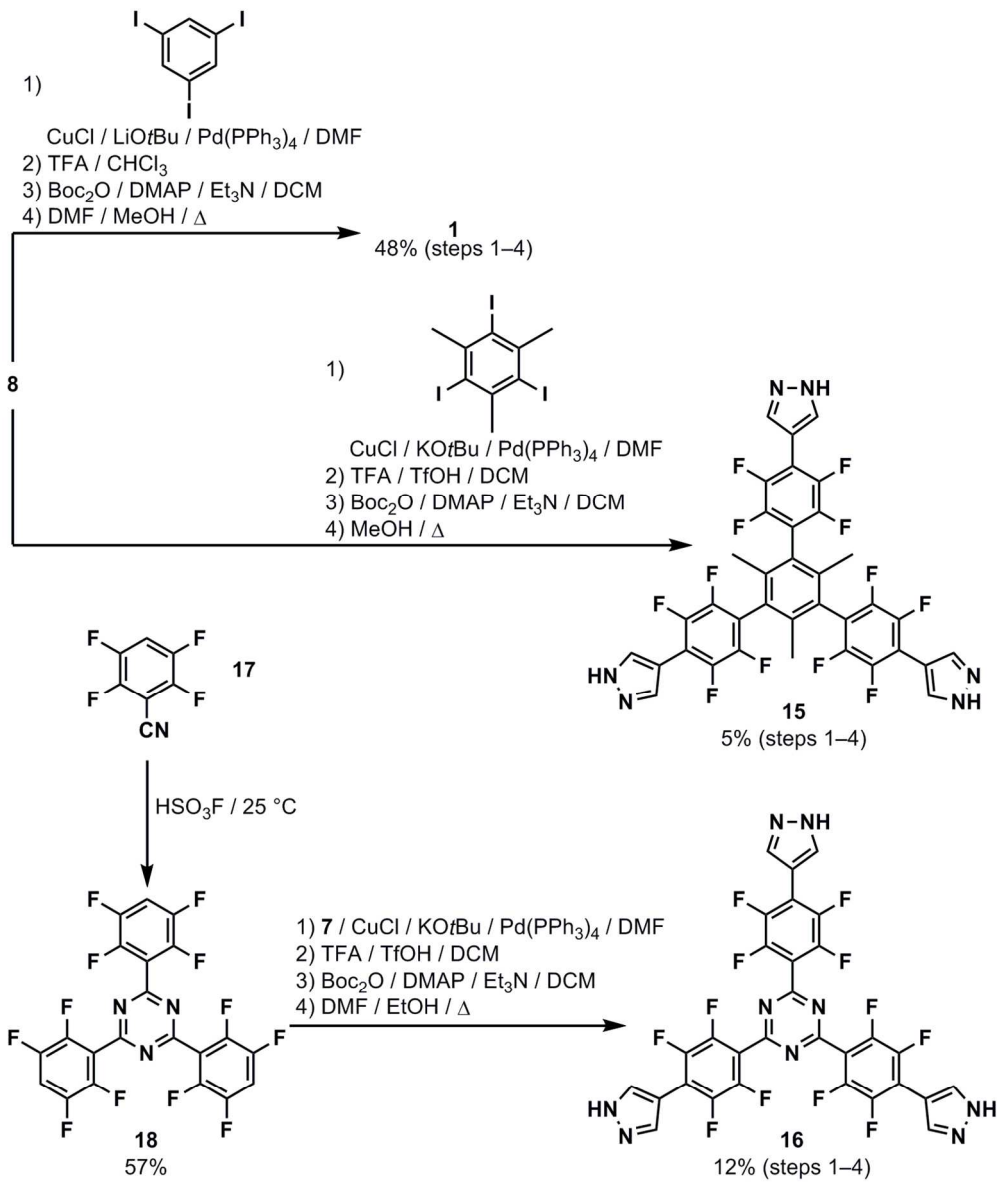

130x154mm (300 x 300 DPI)

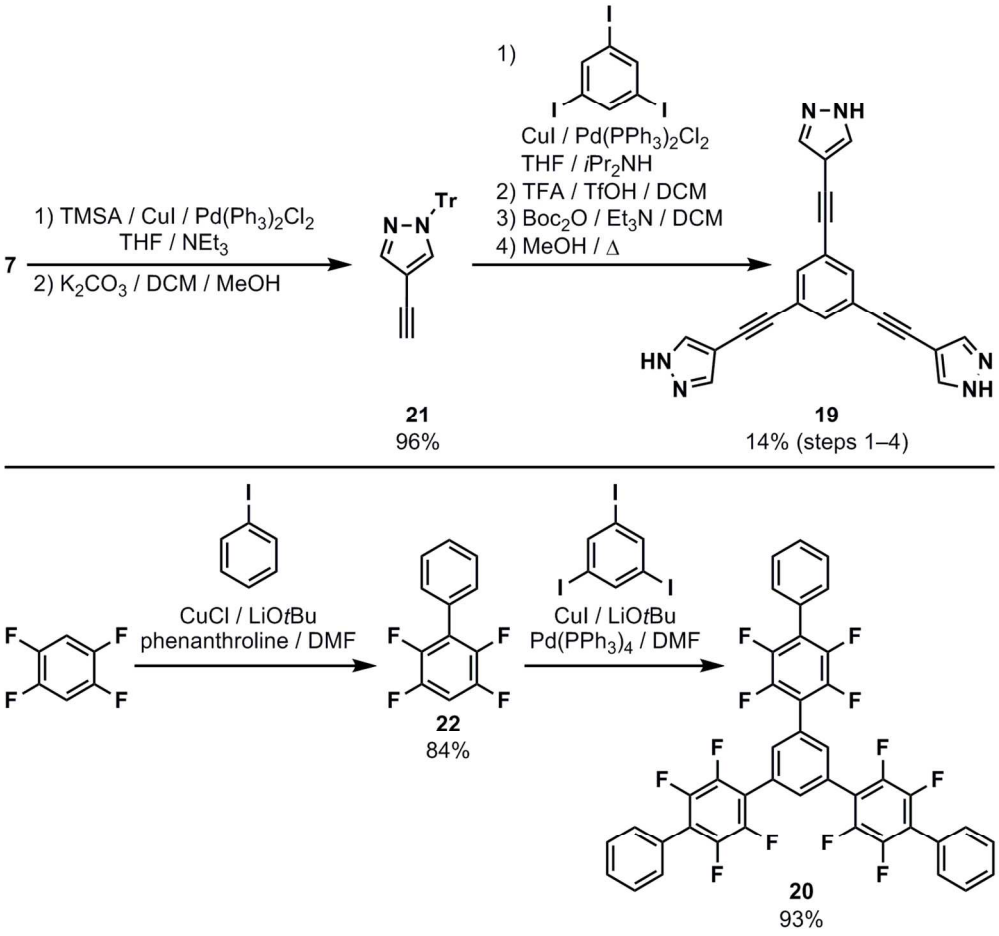

125x118mm (300 x 300 DPI)

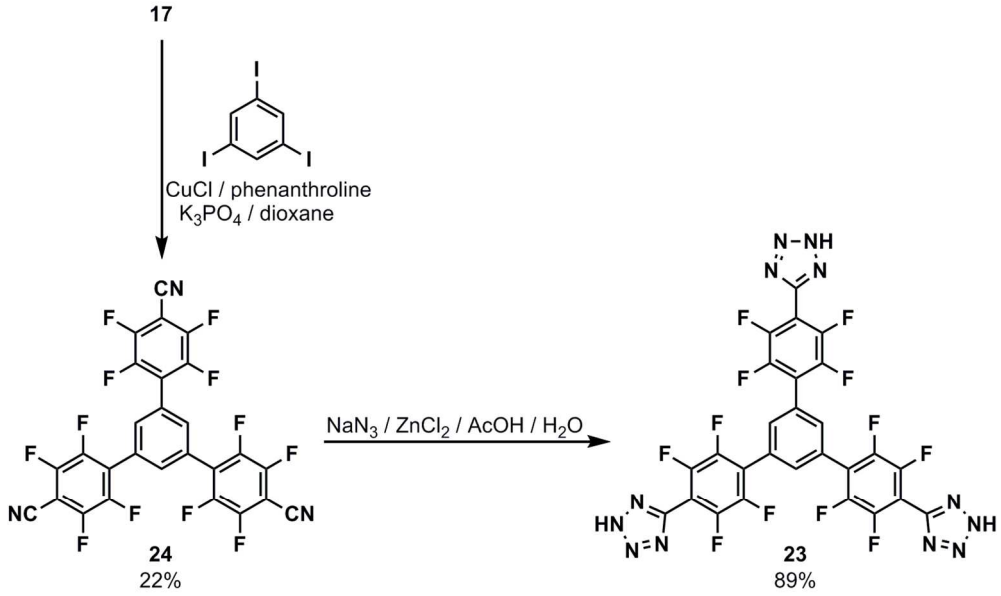

132x79mm (300 x 300 DPI)

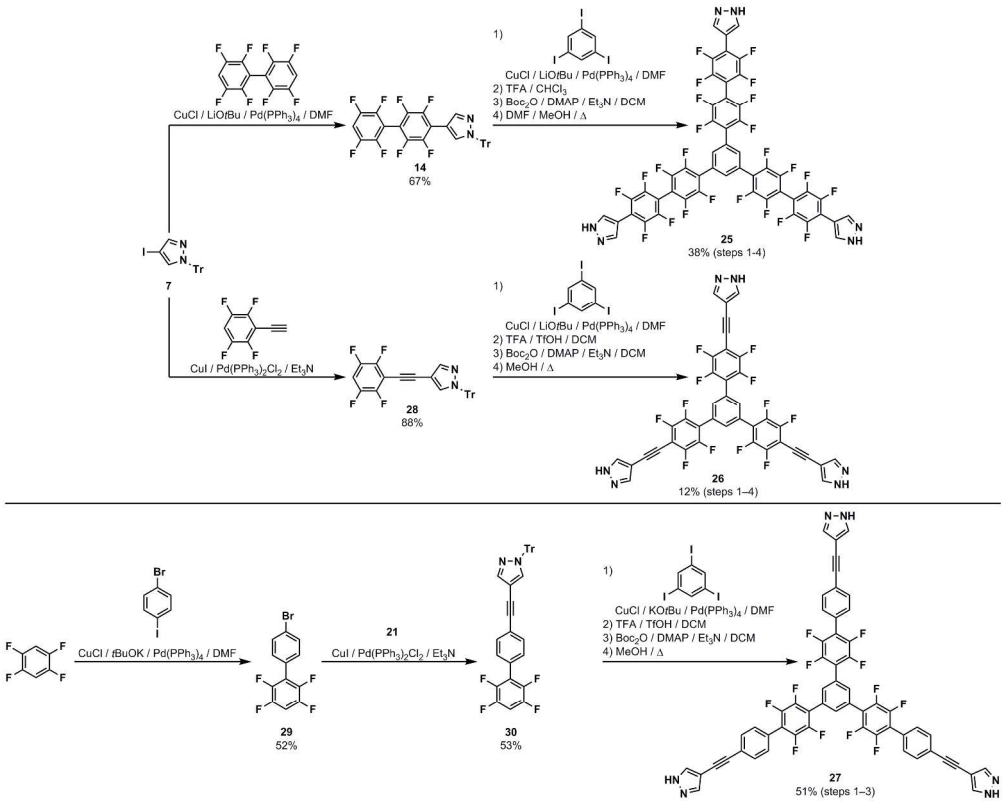

256x204mm (300 x 300 DPI)

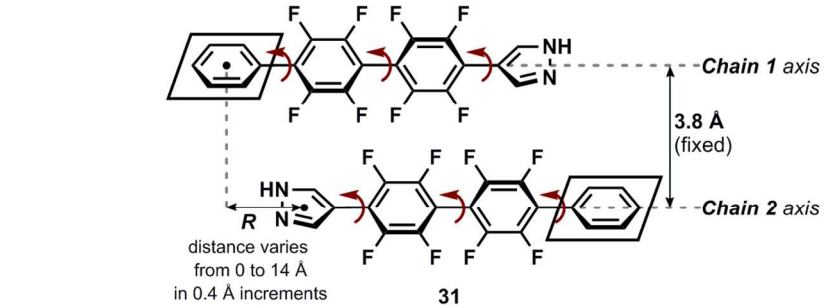

31

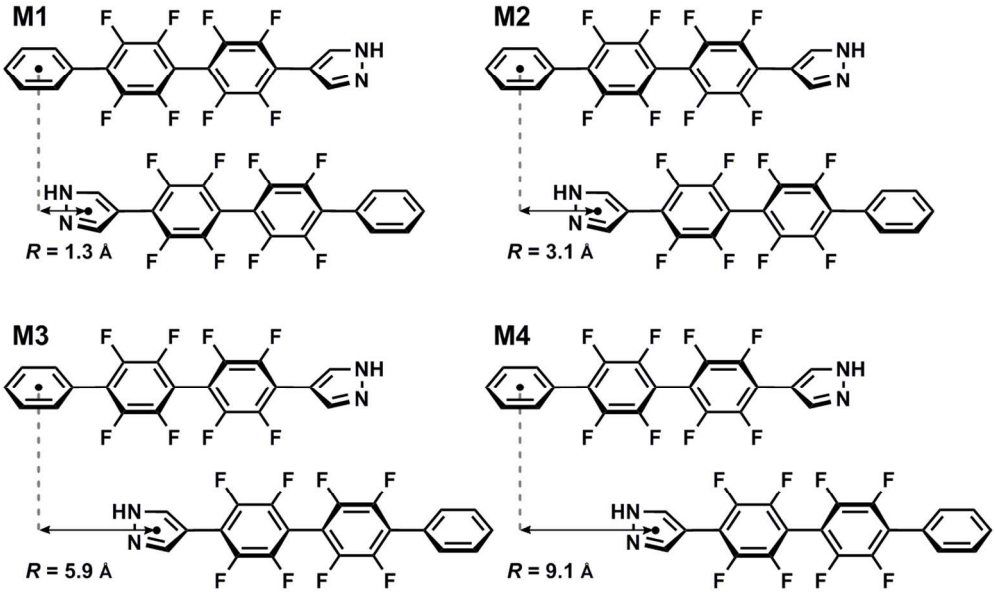

118x110mm (300 x 300 DPI)

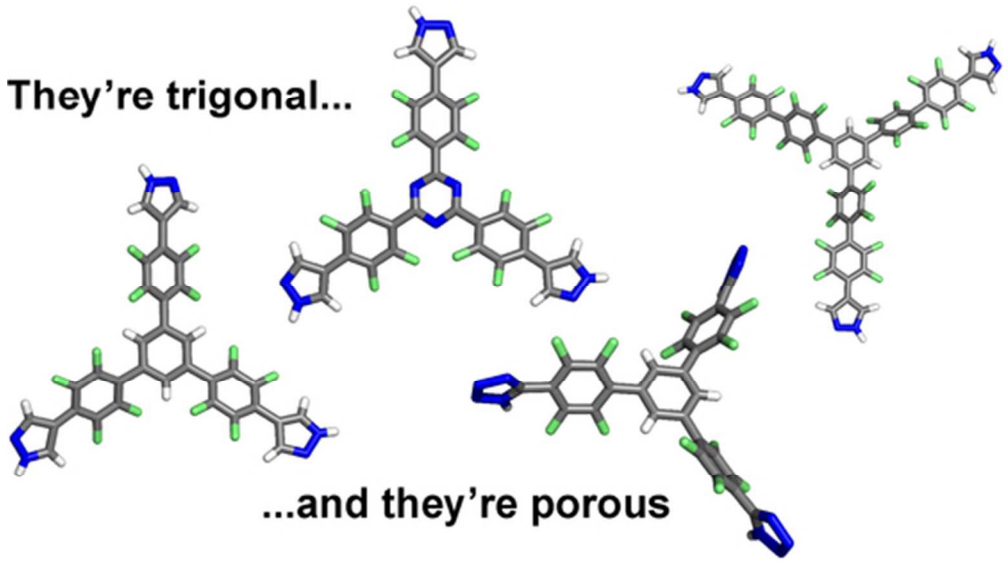

47x26mm (300 x 300 DPI)